Genesis and evolution of regoliths

C. Moragues-Quiroga, J. Juilleret, L. Gourdol, E. Pelt, T. Perrone, A. Aubert, G. Morvan, F. Chabaux, Arnaud Legout, P. Stille, et al.

Catena 149 (2017) 185–198

Contents lists available at ScienceDirect

Catena

journal homepage: www.elsevier.com/locate/catena

Genesis and evolution of regoliths: Evidence from trace and major elements and Sr-Nd-Pb-U isotopes

C. Moragues-Quiroga [a,b,*], J. Juilleret [a], L. Gourdol [a], E. Pelt [b], T. Perrone [b], A. Aubert [b], G. Morvan [b], F. Chabaux [b], A. Legout [c], P. Stille [b], C. Hissler [a]

[a] Catchment and Ecohydrology Research Group (CAT), Luxembourg Institute of Science and Technology (LIST), 41 Rue du Brill, L-4422 Belvaux, Luxembourg
[b] Université de Strasbourg, LHyGeS (UMR 7517 CNRS/EOST/UdS), 1 Rue Blessig, F-67084 Strasbourg Cedex, France
[c] INRA, UR 1138 Biogéochimie des Ecosystèmes Forestiers, Route d'Amance, 54280, Champenoux, Nancy, France

ARTICLE INFO

Article history:
Received 11 February 2016
Received in revised form 14 September 2016
Accepted 18 September 2016
Available online 9 November 2016

Keywords:
Regolith
Sr-Nd-Pb-U isotopes
Trace elements
Mineralogy
Critical zone
Periglacial coverbeds

ABSTRACT

Regoliths encompass different materials from the fresh bedrock to the top of the organic horizons. The occurrence and evolution of these materials are determined by deposition, erosion and weathering processes that are specific for each region. The origin and interaction of the regolith layers are still important issues in the study of critical zone functioning. Studies that attempt to understand the processes responsible for the structure and the evolution of regoliths often focus either on the soil or on the bedrock compartment, and often from a narrowly focused approach using just a single tool such as major element patterns or mineralogy. This limits the understanding of the complete regolith composition and evolution. The present study proposes the combination of mineralogy, major and trace element concentrations, and Sr-Nd-Pb-U isotopes as an extremely useful procedure for tracking the spatial and temporal origin of regolith materials and understanding their stratification. This multi-tracer approach was applied on a regolith profile from the south-western edge of the Rhenish Massif, which is characterised by the occurrence of slate bedrocks and overlying Pleistocene Periglacial Slope Deposits (PPSD). The data allowed the differentiation of three compartments within the regolith: 1) the organic compartment, where low $^{206}Pb/^{207}Pb$ and $^{87}Sr/^{86}Sr$ isotopic ratios reflected the impact of atmosphere-derived components; 2) the PPSD compartment, whose upper horizons were characterised by the presence of atmosphere-derived particles rich in Cd, Sn, Sb, Hg and Pb and by relatively low $^{206}Pb/^{207}Pb$ and $^{87}Sr/^{86}Sr$ ratios, whereas the lower horizons showed Nb enrichments in their matrix and a mineralogical composition pointing to ancient volcanic events; and 3) the weathered slate compartment, whose weathering progression and genetic relationship with the PPSD were particularly well tracked with $^{87}Sr/^{86}Sr$ and $^{143}Nd/^{144}Nd$ isotope ratios, ($^{234}U/^{238}U$) activity ratios and positive Ce anomalies. The results prove the efficiency of radiogenic isotope measurements combined with the analysis of major and trace elements to complete regolith studies. Moreover, these isotopes and elements are shown to be potential geochemical tracers of exchange processes at the water-mineral interface. This approach allows for the first time the description of an evolution scheme of a complete slate regolith, which covers a large part of the Rhenish Massif.

1. Introduction

Regolith represents the unconsolidated mantle of weathered rock and soil material on the Earth's surface (Soil Science Glossary Terms Committee (SSGT), 2008). In a broader sense, it encompasses all material from fresh rock to the atmosphere (Eggleton, 2001; Scott and Pain, 2008; NRC, 2001; Field et al., 2015). Regolith is a major compartment of the critical zone where fluxes of water, energy, solutes and matter occur. The production of regolith from the original bedrock influences the chemistry of surface waters and buffers the atmospheric CO_2 concentration (Banwart et al., 2011; Berner and Maasch, 1996; West et al., 2013). The regolith is the terrestrial environmental compartment where most of the water exchanges occur. Its bio-physico-chemical properties drastically impact the water that percolates and/or stores in its different parts (organic and mineral soil horizons, weathered bedrock, *etc.*).

On a large scale from a space and time perspective, most of the *in situ* regolith systems are polygenetic. As an example, Felix-Henningsen (1994) showed that in the Rhenish Massif a weathering mantle representing the *in situ* regolith with a thickness up to 150 m was formed under warm and humid climates over a long period of time, from the Upper Mesozoic to the Tertiary. Additionally, loose materials produced in the *in situ* regolith move during erosion processes and contribute to form a *transported* regolith after redeposition. This means that

* Corresponding author.
E-mail addresses: cristina.moragues@list.lu (C. Moragues-Quiroga), legout@nancy.inra.fr (A. Legout), christophe.hissler@list.lu (C. Hissler).

http://dx.doi.org/10.1016/j.catena.2016.09.015
0341-8162/

actual *in situ* regoliths recorded successive weathering and erosion stages (Barbier, 2012). Therefore, *in situ* regoliths can also be considered as polygenetic (Taylor and Eggleton, 2001). In the Rhenish Massif, the soil representing the upper part of the regolith is essentially developed from Pleistocene Periglacial Slope Deposits (PPSD - Kleber, 1997; Semmel and Terhorst, 2010) - also called periglacial coverbeds - that cover the weathered *in situ* regolith to constitute a polygenetic regolith system. These PPSD originate from the combination of atmospheric deposition, solifluction and/or cryoturbation of the former active rock layer during the last glacial period (Kleber, 1997; Semmel and Terhorst, 2010). The distances over which these materials were transported range from a local to regional scale. Hence, the alternation of such contrasting materials creates regolith components which may have a proximal, but not direct, genetic link to the underlying bedrock. Their differentiation in the regolith induced many lithic discontinuities that directly impact the evolution of the regolith and control pedogenesis, water infiltration, interflow and root penetration (Lorz and Phillips, 2006; Völkel et al., 2011).

Atmospheric deposition can significantly contribute to the polygenetic evolution of regoliths and mask the autochthonous contribution coming from the bedrock. On the one hand, atmosphere-derived anthropogenic depositions of trace metals originating from agricultural tillage and fertilization, mining and other industrial activities tend to accumulate in the upper soil layers due to their adsorption by organic matter (Aubert et al., 2002; Hissler and Probst, 2006; Steinmann and Stille, 1997). Stückrad et al. (2010) and Stille et al. (2011) suggested, based on a combined trace element and Pb isotope study, a contribution of regional ore-vein derived elements to a regolith from the south eastern edge of the Rhenish Massif and from the Vosges Mountains in France, respectively. On the other hand, loess that was deposited during the Pleistocene is widespread throughout Europe. These deposits form a more or less continuous belt along a 2000 km east-west transect from Great Britain and Brittany in northern France to the Dnieper Valley in Ukraine (Catt, 1986; Paepe and Sommé, 1970; Rousseau et al., 2013, 2014). The origin of the European loess is still a matter of discussion. Nevertheless, Sr and Pb isotopic data clearly demonstrate that the sources of the loess deposits are proximal and different for each region (Rousseau et al., 2014). Some of these aeolian deposits present a typical volcanic mineralogical contribution (Kleber and Terhorst, 2013; Pissart, 1995; Semmel and Terhorst, 2010). Impacts of different Pleistocene volcanic eruptions were identified in the upper layers of the western European regoliths and can serve as efficient chronostratigraphic markers of these systems (Wörner and Schmincke, 1984; Pouclet and Juvigne, 2009; Pouclet et al., 2008). The studies of Gallet et al. (1998) and Chauvel et al. (2014) confirm an earlier conclusion reached by Taylor et al. (1983), that most of these aeolian deposits reflect the chemical composition of the upper continental crust.

The matter and energy exchanges in the critical zone are partly controlled by the structure and evolution of the regoliths; therefore it is especially important to look at the entirety of the regolith when more than one formation occurs in the same profile. Relevant tools are required to improve the understanding of complex critical zone processes and to investigate this hidden part of the ecosystems. Over the last decades, radiogenic isotope, trace element and mineralogical analyses have become state-of-the-art tools for the characterisation of deposit and regolith formations (Debajyoti et al., 1967; Faure, 1986; Michard et al., 1985; Taylor and McLennan, 1981). Sr, Nd, Pb and U isotopes together with trace and rare earth element (REE) distribution patterns have been shown to be very suitable tools to answer open questions about regoliths formation (Aubert et al., 2001; Dequincey et al., 2002; Hissler et al., 2015; Stille et al., 2009, 2011). However, these techniques are rarely applied concurrently.

In the present study, we combine mineralogical, major and trace element and Sr-Nd-Pb-U isotope analyses in order to reach a more comprehensive characterisation of a regolith profile. Our objective is to distinguish the different regolith strata by assessing their origin and evolution, and by evaluating the chemical and isotopical impact between the different strata. Hereby, we also address the question, how far dust from the late-Pleistocene volcanic eruption reached the south-western edge of the Rhenish Massif and mixed with the local loess deposits. To our knowledge, this is one of the few existing studies on a whole regolith system using such a multi-tracing approach.

2. Geomorphology and geological settings

The study site is a 4 ha beech (*Fagus sylvatica* L.) and oak (*Quercus petraea* (Matt.) Liebl.) dominated plateau located at an average altitude of 512 m asl in the Luxembourg Ardennes Massif (Oesling), close to the Belgian border (latitude: 49° 50′ 05.5″N; longitude: 05° 47′ 47.6″E) (Fig. 1). The studied plateau is assumed to be representative of the regolith landform unit called “haute surface de l'Oesling” in Luxembourg, which developed at 500 m asl (Désiré-Marchand, 1985). A regolith landform unit represents an area characterised by similar landform and regolith attributes (Eggleton, 2001). Indeed, landforms are used as surrogates for mapping regoliths since both are usually spatially and genetically related (Craig et al., 1999). This “haute surface de l'Oesling” is the Luxembourg part of an extensive Dano-Montian surface of the eastern part of central Ardennes and Eifel at altitudes above 500 m (Demoulin, 2003) and correlates in Germany with the mapped “S2” surface, developed by pedimentation under semi-arid climate during the Upper Eocene/Lower Oligocene (Huguet, 1998). Désiré-Marchand (1985) explained that this “haute surface” was generated by gradual redevelopment of the original flat surface (S1 surface) and, consequently, the above *in situ* regolith recorded many weathering stages during the geological times and can be considered polygenetic.

The geological substratum of the studied plateau is composed of Devonian metamorphic schists, phyllites and slates (Juilleret et al., 2011) covered by Pleistocene Periglacial Slope Deposits (PPSD), which have been recognized to be the parent material of the soil in the Rhenish Massif (Müller, 1954; Deckers, 1966; Kwaad and Mücher, 1977; Sauer, 2002; Sauer et al., 2002a; Sauer and Felix-Henningsen, 2006). PPSD generally consist of up to 3 different layers, with great variability in the occurrence and thickness of the layers depending on the geographical and topographical location (AG (Ad-hoc-Arbeitsgruppe) Boden, 2005; Dietze and Kleber, 2010; Semmel and Terhorst, 2010), and can be described as follows:

– an upper layer (UL) found in every topographic position. This layer always contains admixed loess and presents a homogenous thickness of 30 to 70 cm. This layer is characterised by higher silt content in comparison to the underlying soil.

– an intermediate layer (IL) which contains rock fragments originating from the bedrock below and also loess, as its presence is strongly controlled by topography and bound to sites especially prone to loess deposition.

– a basal layer (BL) composed almost exclusively of bedrock fragments present in the surrounding slopes. During the formation of the basal layer, bedrock and periglacial debris formed the surface before the onset of loess accumulation. The BL is therefore almost free of allochthonous material like loess and varies greatly in thickness. Rock fragments are usually oriented parallel to the slope and may appear in multiple layers.

According to Dietze and Kleber (2010), the above described layers form a continuous drape in Central European subdued mountains like the Rhenish Massif and may occur as a complete series of 3 layers (UL-IL-BL) or may be reduced to only upper and basal layers (UL-BL). The latter sequence (UL-BL) is the most widespread (Sauer and Felix-Henningsen, 2006).

3. Methodological approach

3.1. Regolith stratigraphy and classification

Prior to the sampling, the studied regolith profile was observed and described (i) from a soil pit for the upper part (0 to 140 cm depth); and

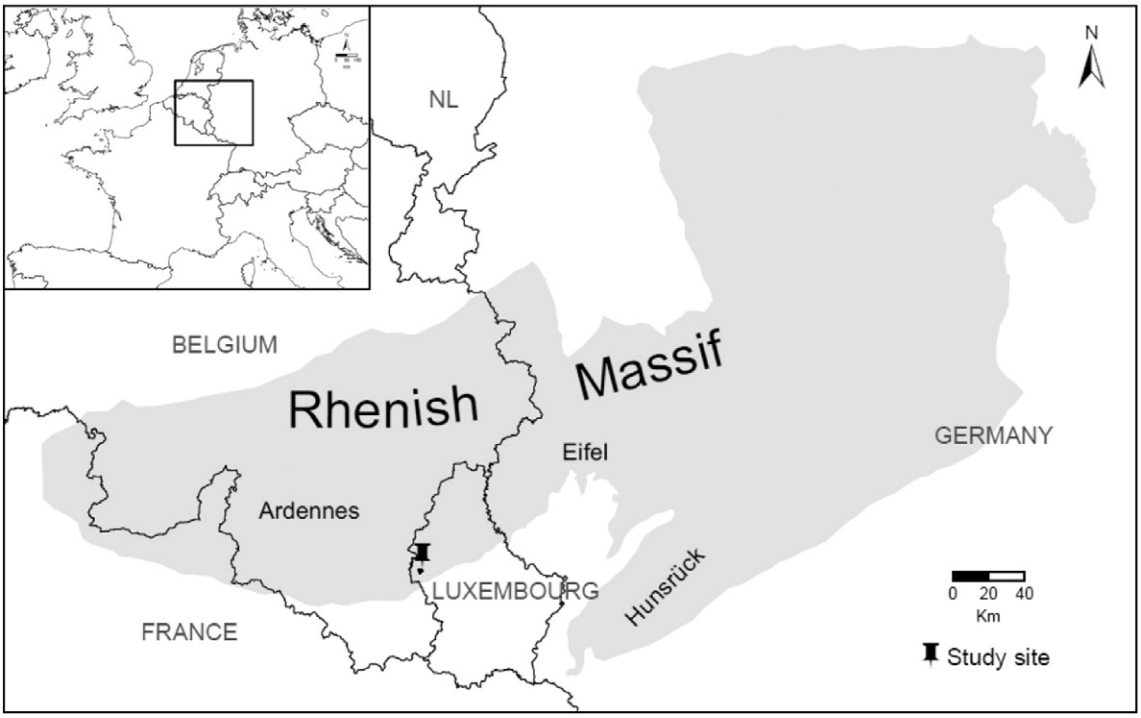

Fig. 1. Situation and extension of the Rhenish Massif in Europe and location of the study site in the Luxembourg Ardennes region.

(ii) by core drilling for the deeper part (140 to 735 cm depth). The following description was made according to the Guidelines for Soil Description (FAO, 2006) and completed with the description of the *subsolum* material according to Juilleret et al. (2016). As regolith encompasses in its upper parts the *solum* (where pedogenic processes and biota are dominant) and in its lower parts the *subsolum* (where the original rock structure or fabric of the Bedrock is preserved), we described and subdivided the profile according to *solum* and *subsolum* parts following the methodology of Juilleret et al. (2016) (Table 1).

The *solum* (from −1 to 45 cm) showed 3 horizons described as follows (Table 1): a very thin layer of fresh to highly decomposed organic material (O horizon) on top of a thin very dark greyish brown (10YR 3/2) silty clay Ah horizon and a brownish yellow (10 YR 6/6) silty clay loam B Cambic horizon. Both organo-mineral horizons were not sticky, non-plastic and showed a soft dry consistency. We estimated fine and very fine root density on vertical plane at 8 to 16 roots cm^{-2} for Ah and B horizons. No earthworm channels were observed. Rock fragments of slate nature and of fine-to-medium gravel size (2 to 20 mm) were common in the Ah and B horizons with respective volume contributions of 13% and 27%.

The upper *Subsolum* (45–140 cm) observed from the soil pit (Table 1) is represented by: an olive yellow (2.5 Y 6/8) loam 2Cg1 horizon, and an olive yellow (2.5 Y 6/6) sandy loam 2Cg2 horizon. The estimated root density on the vertical plane was below 8 roots cm^{-2} in both C layers. The stone content increases significantly in these two horizons and ranges from 40% to 50% of the volume for the respective 2Cg1 and 2Cg2 horizons. Common faint mottling of medium size and a few soft iron-manganese-oxide traces in the earth material around rock fragments were observed. This upper *subsolum* is defined as *Regolithic* layer (Juilleret et al., 2016).

The colours of the deeper *subsolum* material (140–735 cm) ranged from light grey (2.5 Y 7/2) to brownish yellow (10YR 6/6). *Gleyic* properties were observed between 340 and 380 cm depth (WRB, IUSS Working Group, 2015). As the material was mechanically weakened by water, we classified it as *saprolithic* (Juilleret et al., 2016). From 450 to 735 cm depth, the material consisted of longer intact slate rock cores of several centimeters length (5 to 7 cm) mainly of grey colour (GLEY 1 5/N). Some of the longer cores showed cracks covered by sesquioxydes interpreted as a mechanical weakened part inherited from the cleavage planes where waters flow. This deeper material is classified as *paralithic* according to Juilleret et al. (2016).

The abrupt increase and the change in size of rock fragments between B and 2Cg1 horizons allowed us to diagnose a lithic discontinuity. The irregular orientation of the longer axes of slate rock fragments inherited from the underlying geological substratum in the 2Cg1 and 2Cg2 layers were interpreted as indications of cryoturbation. Below the 2Cg2 layer, the observation of the cores from the deeper *subsolum* showed that rock fragments have a different orientation, mainly vertical. The orientation of the slate rock fragments is inherited from the almost vertical cleavage planes of the geological substratum (Juilleret et

Table 1
Regolith structure and stratigraphic characterisation, including location of the samples (LD: lithic discontinuities; UL: upper layer; BL: basal layer).

Stratigraphy	Regolith profile		Horizons layers	Diagnostic material	Sample depth (cm)	Sample name	
PPSD (LU)	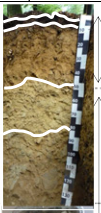	Solim	O		−1 – 0	OH	
			Ah		0 – 4	PPSD1	
			B	Cambic	4 – 45	PPSD2	L.D
PPSD (BL)			2Cg1	Regolithic	45 – 80	PPSD3	
			2Cg2	Regolithic	110	PPSD4	L.D
Slate substrate		Subsolum	3CR	Saprolithic	190	SP1	
			3CR	Saprolithic	270	SP2	
			3CR	Saprolithic	320	SP3	
			3CR	Saprolithic	380	SP4	
			3R	Paralithic	735	SP5	

al., 2011). This observation allows us to diagnose a lithic discontinuity between the 2Cg2 horizon and the geological substratum 3CR layer below.

According to the PPSD classification, we concluded that Ah and B horizons developed in the UL. Indeed, Ah and B horizons present a higher silt content with a cumulate thickness of 45 cm, while the underlying 2Cg1 and 2Cg2 are characterised by a dominant amount of rock fragments originated from cryoturbation. Consequently, the studied profile presents a *transported* regolith part made of PPSD on top of the *in situ* slate weathered substratum and is organized as follows (Table 1):

1) An organic topsoil, which encompasses the O horizon and constitutes the upper part of the *solum*.
2) An organo-mineral compartment developed in the PPSD which can be subdivided in *solum* and upper *subsolum*. The *solum* part is composed of Ah and B horizons. The upper *subsolum* can be divided into 2Cg1 and 2Cg2 horizons and contains *regolithic* material according to Juilleret et al. (2016).
3) A lower mineral *subsolum*, which contains *saprolithic* and *paralithic* materials according to Juilleret et al. (2016). This third compartment represents the *in situ* regolith profile made of weathered slate substratum and referred to as 3CR and 3R layers. These layers are separated from the above PPSD compartment by a lithic discontinuity.

The studied regolith profile can be classified as Haplic HEMIMODER (Jabiol et al., 2013) developing on a Dystric Cambisol (Ruptic, Endoskeletic, Siltic, Protospodic) (IUSS Working Group, 2015) overlying a Regolithic Saprolite (Gleyic, Ruptic, Rootic, Siltic, Skeletic) [Slatic] (Juilleret et al., 2016). In order to simplify the presentation of the results and the discussions, the name of the samples of the regolith layers (Table 1 – OH, PPSD, SP) will be used in the following document as reference of the regolith compartments.

We fulfilled the same pedo-stratigraphic report for four other profiles in the same plateau area. We searched for a profile that minimized the effect of erosion of the plateau unit ("haute surface de l'Oesling") and permitted thicker layers to be investigated. Given the homogeneity we observed *in situ* and in later chemical analyses, this extensive sampling allowed us to choose the studied profile as a representative example of the geological system, on which we therefore focus this work.

The profile description is considered as a general framework that, although very informative, does not allow by itself the distinction of the origin of the various contributions to the regolith composition, for which geochemical analyses are needed. Indeed, the pedo-stratigraphic study informs about the physical properties of the material and its position within the regolith profile. But, this does not yield any precise information about in how far the *in situ* soil has been modified by external contributions such as aeolian depositions (loess or volcanic dust). In addition, only geochemical and isotopic investigations allow us to understand the chemical evolution of the different parts of the regolith.

3.2. Samples collection and preparation

The sampling strategy was based on the description of the entire regolith presented above. We collected samples from the regolith profile including organic, organo-mineral and mineral material in three different steps from the surface to the deeper layers. First, we manually collected the highly decomposed organic material of the OH topsoil horizon on a 4 m^2 area around the opened soil pit in order to obtain a sufficient volume for further analyses. Second, we performed a soil sampling from the soil pit according to the ISO 10381 guidelines for soil sampling. Special attention was given to collect a representative amount of material for each horizon. According to the stone content, we collected 5 to 10 kg of material for each layer and homogenized it prior to taking representative aliquots for the laboratory analyses. Third, we sampled five layers from the core drilling from 140 cm depth (weathered slate) to 735 cm depth (fresh slate bedrock). We encountered some difficulties in obtaining continuous cores as the technique used requires water flow to remove cuttings (Gabrielli and McDonnell, 2012). The material extracted from 140 to 450 cm was made of pieces of rock fragments with muddy matrix. All the samples were stored in plastic bags and air-dried in the laboratory before being prepared for analyses.

We sieved the organic topsoil sample to 1 mm in order to remove the coarse vegetal debris that could remain after the sampling of the OH horizon. Then we fully ground it to 63 μm in a Fritsch centrifugal ball mill Pulverisette 6 in order to homogenise potential semi-decomposed organic particles. We sieved the *solum* and upper *subsolum* first at 2 mm in order to separate the coarse elements (>2 mm fraction), composed of slate rock fragments, and the fine earth (<2 mm fraction), called PPSD matrix in the manuscript. A representative aliquot of coarse elements (PPSDce) was separated and ground to 63 μm. Then, the fine earth was sieved at 63 μm for the mineralogical and chemical characterisation of the PPSD matrix. The material collected from the core drillings (lower *subsolum* samples - SP samples) was ground to 63 μm in a Fritsch centrifugal ball mill Pulverisette 6.

3.3. Analytical methods

We analysed aliquots of all regolith powdered samples for mineralogical contents by X-Ray Diffractometry (XRD, diffractometer RX Bruker, D5000) and Scanning Electron Microscopy (SEM, TESCAN Vega II fitted with EDAX X-ray energy dispersive spectrometer). We used Inductively Coupled Plasma – Optical Emission Spectrometry (ICP-OES, Thermo Fischer ICap 6500) and Inductively Coupled Plasma – Mass Spectrometry (ICP-MS, Thermo Elemental X7/Perkin-Elmer© DRC-e) for determining major and trace element concentrations respectively for all samples after digestion by $LiBO_2$ alkaline fusion. The analytical errors were <5% for both instruments.

Regolith sample aliquots used for isotopic composition analyses were preliminary digested using HNO_3:HF:$HClO_4$ concentrated acid mixture in Savillex® Teflon vessels. We separated Sr, Pb and Nd from other elements for radiogenic isotope analyses by extraction chromatography on Eichrom Sr Spec, TRU Spec and Ln Spec resins, respectively, following the procedures of Geagea et al. (2007) and Guéguen et al. (2012) adapted from Pin and Zalduegui (1997) and Deniel and Pin (2001). U was separated by chromatography on Biorad AG1x8 anionic resin following procedures developed at the LHyGeS (Strasbourg, France) (Chabaux et al., 1997; Dequincey et al., 2002; Granet et al., 2010; Pelt et al., 2008). We measured Sr and Nd isotopic ratios on a Thermo-Scientific Triton (TIMS) and Pb and U isotopic ratios on a Neptune Thermo-Scientific multicollector (MC-ICP-MS). Mass fractionation of Pb isotopic ratios was corrected online using a SRM 997 Tl isotopic standard following the procedure of the laboratory (Stille et al., 2011). Mass fractionation and the Faraday/SEM drift during U isotopic measurements by MC-ICP-MS were corrected by bracketing against the IRMM-184 natural U standard. The 2014 mean for the Sr SRM 987 standard yields a $^{87}Sr/^{86}Sr$ ratio of 0.71025 ± 0.00002 (2SD, n = 21) and for the La Jolla standard a $^{143}Nd/^{144}Nd$ ratio of 0.511842 ± 0.000006 (2SD, N = 7). The Pb SRM 981 standard measurement during the session gave the following ratios: $^{208}Pb/^{206}Pb$ = 2.16604 ± 0.00002, $^{207}Pb/^{206}Pb$ = 0.914651 ± 0.000007, $^{206}Pb/^{204}Pb$ = 16.9267 ± 0.0004 (2SE), which are within the 2014 0.2‰ dispersion observed in the lab and consistent within <1‰ with the reference values of Doucelance and Manhès (2001). The HU1 uraninite was measured 5 times during the uranium MC-ICP-MS session and yields a ($^{234}U/^{238}U$) activity ratio of 0.9983 ± 0.0004 (2SD) consistent with secular equilibrium within 2‰. The analysis of the ID-blanks suggests a contamination of <30 pg for Sr and Nd, ~ 400 pg for Pb and 23 pg for U which is negligible compared to the amount processed (>200 ng of Sr, Nd, Pb and U for all samples except for the humus sample with 20–30 ng U).

3.4. Statistical methods

In order to determine groups of major and trace elements that follow similar variation patterns in the regolith with depth, we performed a hierarchical cluster analysis (*e.g.* Hartigan, 1975; Kaufman and Rouseeuw, 1990; Kaufman and Rousseeuw, 2005). Such statistical technique has been widely used for drawing meaningful information from geochemical data (*e.g.* Bini et al., 2011; Levitan et al., 2015; Schot and van der Wal, 1992). For the linkage rule, we chose the Ward's method (Ward, 1963), which has been successfully used in many previous studies (Gourdol et al., 2013; Lin et al., 2014). For the linkage distance, the Pearson correlation distance (1 – Pearson correlation coefficient) was retained, which is suitable for clustering variables (Reimann et al., 2008). Prior to the analysis, the most universal z-transformation was applied to each parameter (mean subtraction and division by standard deviation) to ensure that each major and trace element is weighted equally (Templ et al., 2008). The resulting dendrogram, illustrating the similarity of the parameters, was cut using two phenon lines to define groups and subgroups of parameters. Defining the number of groups by selecting the position of the phenon line up or down the dendrogram is a subjective evaluation step (Güler et al., 2002). The heights of these two phenon lines were retained by visual inspection of the dendrogram and the associated ordered z-transformed concentrations matrix and gave us the most satisfactory geochemical parameters groups and subgroups in terms of variations with depth.

4. Results

4.1. Mineralogical composition of the regolith components

The XRD analyses (Fig. 2) indicate that PPSD3 and PPSD4 are enriched in phyllosilicates and clay minerals, mainly chamosite, a Fe-rich polytype of chlorite, and kaolinite. At these depths, chamosite and kaolinite show relative abundances ranging from 17 to 20%. Other chlorite polytypes are much less abundant (rel. abund. <3%). The illite/mica group shows increasing abundances with depth in the matrix of the PPSD compartment between 7 and 28%. Similarly, one observes enrichments in orthoclase (rel. abund. 8%) in PPSD3 and PPSD4 and in albite (3%) at the PPSD2 and PPSD3 layers. Conversely, anorthite is depleted between PPSD2 and PPSD4 (rel. abund. <3%), and quartz is depleted at the PPSD3 and PPSD4 layers (rel. abund. 16 to 24% respectively), both compared to the above *solum* horizons (PPSD1 and PPSD2) and the *subsolum* saprolithic material below (SP), where the relative abundances scatter between 8 and 11% for anorthite and 36 and 57% for quartz. Rock fragments from the PPSD (PPSDce) generally present a mineralogical composition rather similar to the SP compartment, being slightly more enriched in kaolinite (12%) and notably in orthoclase (14%).

SEM analyses on all PPSD samples indicate that in this compartment there are REE-bearing minerals such as monazite, xenotime, zircon and florencites. Other Ti-bearing and iron oxide trace minerals observed at these depths are rutile, ilmenite and Ti-magnetite.

4.2. Chemical composition of the regolith components

The chemical composition of the entire regolith is shown in Table 2. Na_2O and TiO_2 are enriched in the PPSD matrix between PPSD2 and PPSD4 compared to SP. K_2O, Fe_2O_3, MgO and Al_2O_3 tend to increase with depth within the matrix of the PPSD compartment and reach values similar to those of the underlying saprolite (SP samples). CaO concentrations are high at the OH horizon and decrease with depth in PPSD, showing an important depletion on top of the SP regolith compartment, where it slightly increases again towards the fresh bedrock. On the contrary, P_2O_5 is highly enriched at the top (PPSD1) and bottom (PPSD4) of the PPSD and in SP3 similarly to MnO and Fe_2O_3. PPSDce is, compared to the matrix between PPSD2 and PPSD4, depleted in TiO_2, K_2O and Al_2O_3. PPSDce is enriched in Fe_2O_3 with respect to the rest of the profile, with the exception of SP3. SiO_2, CaO, MgO and MnO show in PPSDce similar concentrations as in the SP1 compartment, whereas Na_2O and P_2O_5 PPSDce concentrations are rather close to the ones of the soil matrix at the PPSD bottom horizons.

The trace elements can be classified in three groups according to the vertical evolution of their concentrations within the regolith profile (Fig. 3). Group I contains Cd, Sn, Sb, Hg and Pb. Their concentrations are higher in the top layer of the PPSD compartment and are low and almost constant throughout the rest of the regolith profile (SP). Group II is composed of Co, Ni, Cu, Zn and As, which present high concentrations in PPSD4 and are enriched in SP3. Group III includes trace elements having increasing concentrations with depth in the PPSD and a notable decrease in the concentrations between PPSD and SP. These elements can be divided in three subgroups according to their behaviour in the SP compartment: Group IIIa encloses those presenting a concentration increase at 380 cm depth, similar to Mg and K (U, Pr, Nd, Gd, Sm, Eu); Group IIIb those that, similar to Al, Si and Ti, remain stable below 200 cm depth (Cr, Rb, Sr, Y, Nb, Th, La Ce, Tb, Dy, Ho, Er, Tm, Yb, Lu) and Group IIIc those that continue decreasing after 200 cm depth, like Na (Zr, Hf).

Major and trace element concentrations of PPSD and SP samples are normalized to the deeper SP lithic material (SP5), which can be considered, at this study site, as the fresh slate (Fig. 4). Compared to this local reference, OH and PPSD1 are depleted in most of the elements, except the trace elements of group I. The other PPSD and SP samples are slightly enriched and show almost identical distribution patterns with ratios close to 1 for most of the analysed elements. However, the enrichments of the elements of Group II in SP3 and SP4, especially Mn, Co, As and U are different. Compared to the slate reference, Nb is generally slightly enriched in the PPSD compartment (ratio = 1.4), whereas the underlying SP samples present a ratio of 1.0. This is also not the case for the rock fragments of PPSD (PPSDce), whose Nb ratio is 0.77.

Post Archean Australian Shale (PAAS) normalized Rare Earth Element (REE) concentrations of PPSD and SP samples show similar

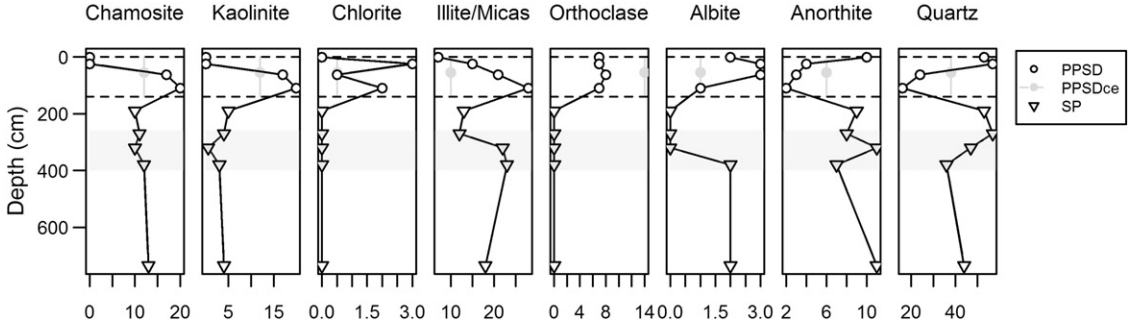

Fig. 2. Depth-dependent patterns of mineralogical composition from XRD analyses expressed in relative abundances (PPSDce: PPSD coarse elements; dashed lines: lithic discontinuities; shaded area: redox sensitive zone).

Table 2
Major (% oxide) and trace element (ppm) composition of the regolith (D.L.: detection limit; NA: not analysed).

	D.L.	OH	PPSD1	PPSD2	PPSD3	PPSD4	PPSDce	SP1	SP2	SP3	SP4	SP5
Major elements (% oxide)												
Na_2O	0.01	0.05	0.24	0.38	0.38	0.40	0.44	0.30	0.21	0.24	0.27	0.26
MgO	0.015	0.10	0.30	1.02	1.69	1.92	1.57	1.90	1.85	1.73	2.18	1.83
Al_2O_3	0.02	1.31	7.70	16.49	19.12	22.86	13.11	19.13	16.69	18.76	20.01	18.29
SiO_2	0.02	<0.02	37.82	62.82	60.27	52.92	66.35	62.51	64.16	58.53	59.41	64.35
P_2O_5	0.04	<0.04	0.27	0.16	0.12	0.22	0.21	0.07	0.17	0.29	0.15	0.15
K_2O	0.01	0.28	1.31	2.63	3.41	3.92	1.96	3.62	3.07	3.72	4.19	3.77
CaO	0.03	<0.03	0.10	0.08	0.05	0.00	<0.03	0.00	0.00	0.04	0.06	0.15
TiO_2	0.02	<0.02	0.55	1.01	1.05	1.12	0.64	0.96	0.86	0.93	0.95	0.87
Fe_2O_3	0.02	0.66	3.48	5.77	6.66	7.99	10.90	5.26	7.15	9.15	6.31	5.56
MnO	<0.001	0.05	0.03	0.06	0.05	0.09	0.05	0.02	0.03	0.94	0.05	0.05
Trace elements (ppm)												
Cr	4	15.4	72.6	127.3	151.6	173.8	120.8	166.9	144.0	144.4	149.8	133.6
Co	0.4	1.7	5.0	15.3	17.5	20.9	20.5	16.0	13.8	200.8	61.9	15.3
Ni	5	8	20	60	71	78	83	74	74	131	79	68
Cu	5	12	20	20	23	39	30	17	41	68	36	44
Zn	11	46	84	145	107	147	110	96	115	175	116	101
As	1.5	2.5	14.9	8.2	9.5	13.8	10.1	8.3	14.9	18.2	12.5	7.6
Rb	0.4	12.2	74.1	159.3	175.6	193.3	91.0	166.6	146.1	167.0	187.7	170.4
Sr	2	14	48	94	110	126	61	96	81	102	113	98
Y	0.2	<0.2	15.8	31.5	38.7	36.6	22.2	34.8	31.8	32.6	33.7	28.0
Zr	1	<1	154	283	305	293	168	260	190	177	174	149
Nb	0.09	<0.09	10.28	19.87	19.44	19.66	10.77	15.96	14.61	14.94	15.28	13.93
Cd	0.12	0.25	0.32	0.25	0.27	0.25	0.2	0.25	0.24	0.28	0.19	0.16
Sn	0.45	0.12	9.63	3.76	4.13	4.63	2.44	4.13	3.72	4.30	4.45	4.04
Sb	0.2	0.4	2.9	0.6	0.5	0.5	0.4	0.3	0.7	0.9	0.7	0.4
La	0.09	2.23	22.03	45.30	51.45	61.33	30.62	48.00	41.00	48.29	57.40	44.04
Ce	0.14	4.26	43.15	91.90	102.90	128.00	61.53	96.75	82.07	109.30	124.10	89.11
Pr	0.015	0.502	4.876	10.340	11.640	14.550	7.052	11.580	9.511	11.880	15.150	10.180
Nd	0.06	1.87	17.93	37.48	42.35	54.10	25.80	43.11	35.83	45.39	59.72	37.89
Sm	0.015	0.313	3.250	6.923	7.778	9.712	4.968	8.233	7.068	9.039	11.680	7.216
Eu	0.005	0.058	0.659	1.408	1.562	1.875	1.030	1.602	1.458	1.871	2.348	1.471
Gd	0.013	0.176	2.682	5.668	6.465	7.161	4.099	6.494	6.111	7.474	8.833	5.970
Tb	0.003	0.029	0.446	0.916	1.074	1.104	0.670	1.001	0.973	1.097	1.187	0.892
Dy	0.01	0.17	2.81	5.80	6.89	6.81	4.11	6.21	5.99	6.50	6.76	5.41
Ho	0.002	0.036	0.601	1.201	1.451	1.395	0.847	1.286	1.250	1.326	1.340	1.112
Er	0.01	0.10	1.63	3.26	3.93	3.79	2.28	3.50	3.32	3.53	3.46	2.94
Tm	0.001	0.016	0.241	0.470	0.571	0.563	0.336	0.512	0.484	0.519	0.506	0.429
Yb	0.007	0.110	1.647	3.274	3.904	3.829	2.296	3.447	3.315	3.531	3.409	2.996
Lu	0.003	0.016	0.252	0.508	0.592	0.586	0.357	0.520	0.500	0.543	0.516	0.451
Hf	0.03	<0.03	3.98	7.53	8.02	7.93	4.55	6.99	5.49	5.16	5.18	4.40
Hg	<0.001	<0.001	0.342	0.091	0.050	0.038	<0.001	<0.001	0.040	0.049	0.043	0.031
Pb	0.7	41.6	128.9	19.4	14.6	14.6	8.9	30.3	24.3	33.7	24.5	17.8
Th	0.06	0.66	7.07	13.21	15.07	17.26	10.12	14.53	13.22	14.43	15.21	13.71
U	0.03	0.33	1.93	3.14	3.14	3.51	2.45	3.09	3.82	5.22	5.84	3.83

distribution patterns (not shown). They display middle REE (MREE) enrichments, which are more notable in coarse materials (PPSDce), in the matrix of PPSD4 and in SP, especially at SP4, as indicated by the $(Eu/Yb)_N$ ratios (Fig. 5). Similarily, though to a lesser extent, $(La/Yb)_N$ ratios point to a strong enrichment of light-REE (LREE) in PPSD4 and SP4, whereas a positive Ce anomaly ($Ce_N/Ce_N^* = 1.05$) is only observable in SP3. Ce is an especially interesting element as it is one of the most reactive REE. Conversely to most of the other REE, it can pass from state 3+ to 4+ and precipitate as cerianite (CeO_2) in oxidizing conditions (Braun et al., 1990). Here, Ce anomalies are calculated as the enrichment of Ce with respect to other LREE (namely La and Pr) normalized to Post Archean Australian Shales (PAAS) with the equation $[Ce_N/Ce_N^* = Ce_N/(0.5La_N + 0.5Pr_N)]$.

4.3. Pb, Sr, Nd and U isotopic compositions of the regolith components

All isotope data are given in Table 3. $^{87}Sr/^{86}Sr$ and $^{206}Pb/^{207}Pb$ ratios are low in OH and PPSD1 (0.7218 and 1.153 respectively) and increase with depth through PPSD2 and PPSD3 up to 0.7387 and 1.220, respectively (Fig. 6a and b). $^{87}Sr/^{86}Sr$ ratio decreases in PPSD4 (0.7366), increases again in the saprolithic material of the SP and has the highest isotopic ratio in the lithic material at SP5 (0.7416). $^{206}Pb/^{207}Pb$ ratio still increases beyond PPSD4 and, after a remarkable decrease at the lithic discontinuity between PPSD and SP, increases again until the deeper part of the regolith (1.214), similar to $^{87}Sr/^{86}Sr$. The coarser materials of the PPSD (PPSDce) display $^{87}Sr/^{86}Sr$ ratios close to the values of the lower PPSD (0.73736) and high $^{206}Pb/^{207}Pb$ ratios compared to both PPSD and SP compartments. The $^{143}Nd/^{144}Nd$ ratios show rather small variations between 0.51192 and 0.51198 throughout the profile (Fig. 6c). The ratio is slightly higher for the OH horizon (0.51195) compared to the other soil horizons (0.51192).

The ($^{234}U/^{238}U$) activity ratios scatter between 0.947 and 0.960 along the profile with the exception of the 270 and 320 cm depth horizons. At these depths, SP2 and SP3 show ($^{234}U/^{238}U$) activity ratios higher than 1 (1.05 and 1.04 respectively - Fig. 5d).

5. Discussion

5.1. Major and trace element behaviour within the studied regolith system

The cluster analysis on the PPSD matrix and SP samples indicates that there are three groups of elements that have different origins and contrasted behaviours during weathering and pedogenetic processes (Fig. 3). Even though the coarse elements of the PPSD are not included in this statistical assessment, and thus uncertainty increases, the results

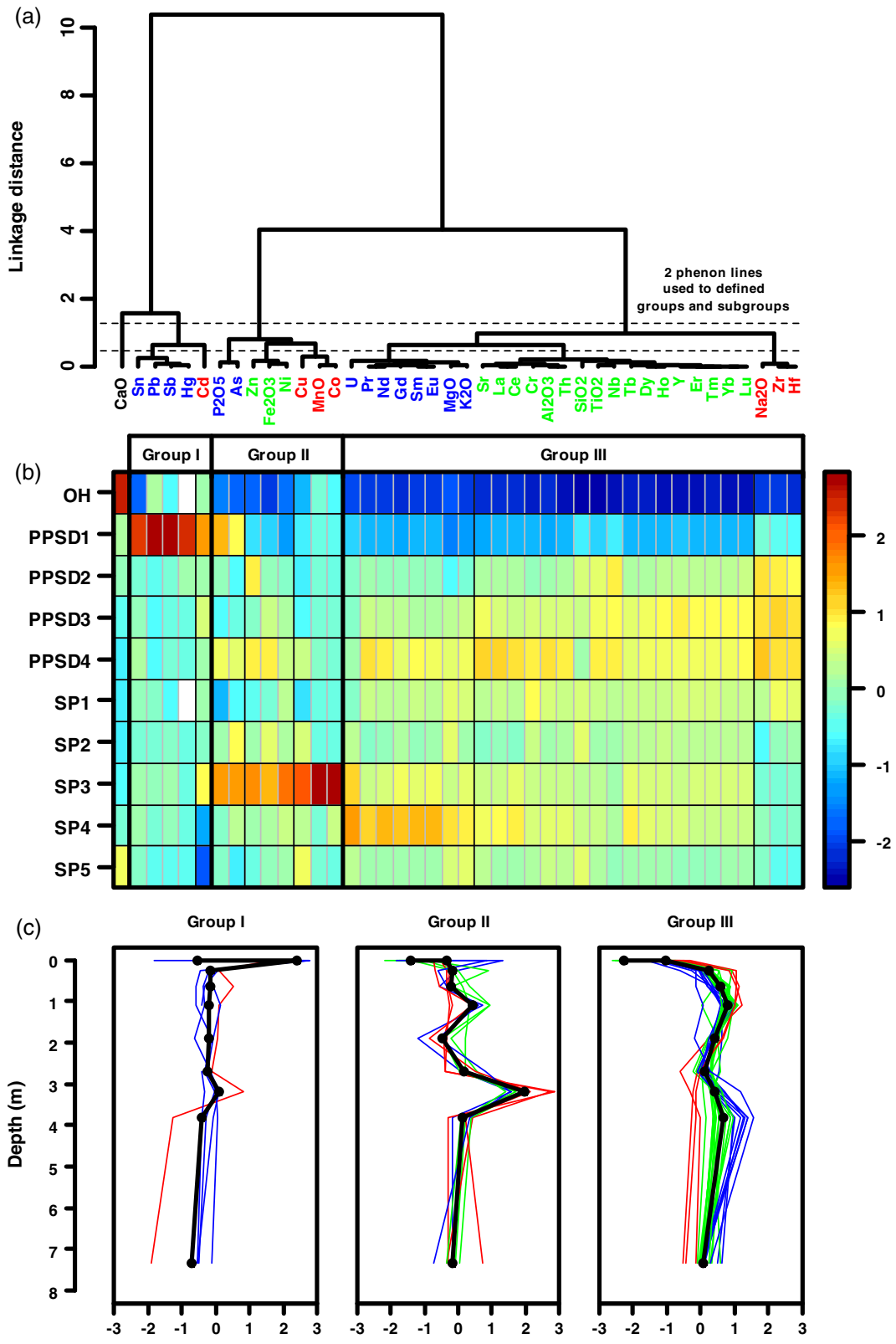

Fig. 3. Hierarchical cluster analysis performed on major and trace elements: (a) dendrogram defined using Pearson correlation distance as distance measure and Ward's method for the linkage rule; (b) coloured z-transformed concentrations matrix (row names correspond to regolith layers, parameter columns are ordered as the dendrogram); and (c) z-transformed concentrations as a function of depth for the 3 parameter groups defined (the thick black lines correspond to the median of each group, the thin coloured lines correspond to individual parameters of each subgroup as defined by the colour of the parameter labels in the dendrogram (a)).

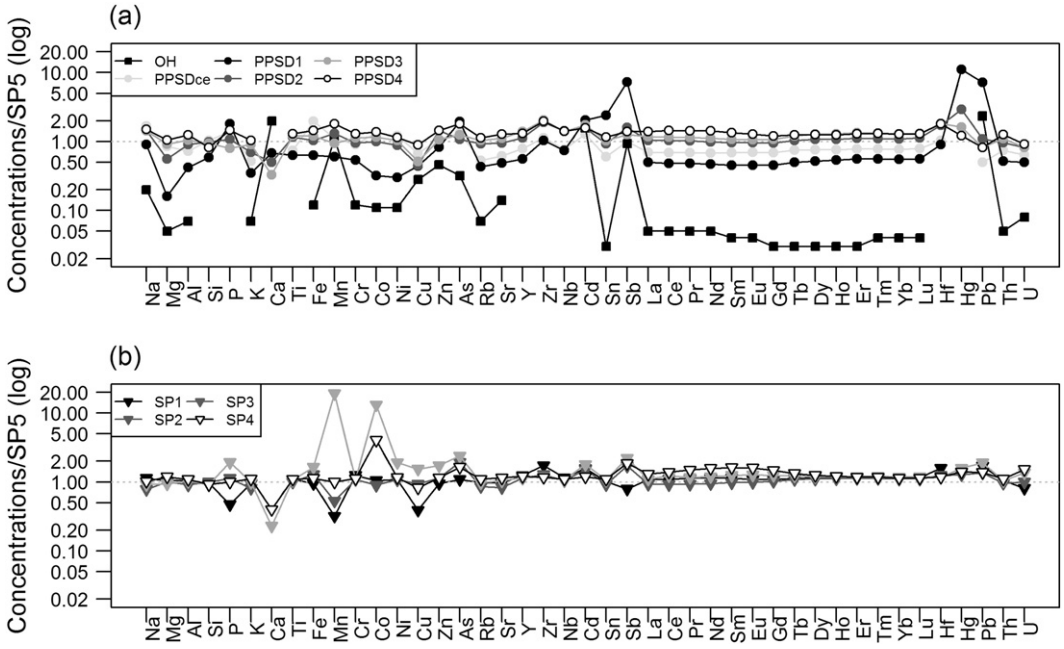

Fig. 4. Major and trace element concentrations of (a) OH and PPSD samples and (b) SP samples, normalized to the SP5 sample concentrations, representing the fresh slate bedrock.

allow discerning the chemical zonations according to the soil fraction that is responsible for most of the processes described below.

Group I includes elements such as Cd, Sn, Sb, Hg and Pb, which are only enriched in the surface Ah horizon (PPSD1) and are probably atmosphere-derived and of anthropogenic origin. The Ah horizon is located directly under the organic horizon (OH) and is as a consequence rich in organic matter, which is known to trap heavy metals and subsequently release them by leaching into the soil (Hissler and Probst, 2006; Steinmann and Stille, 1997; Stille et al., 2009, 2011). This is especially observable in the Pb isotope data (Fig. 6). According to the work of Redon et al. (2013), depth patterns of Sn, Sb, Hg and Pb present a disconnection between upper soil horizons and the rest of the regolith as well as the PPSD coarse materials (PPSDce; Table 2), supporting the hypothesis that they do not derive from the underlying saprolite but from the atmosphere. In contrast is the slight Cd enrichment at 320 cm depth (SP3) compared to the horizons underneath, which resembles that of the elements of Group II and thus cannot be attributed to anthropogenic deposition at the top of the regolith.

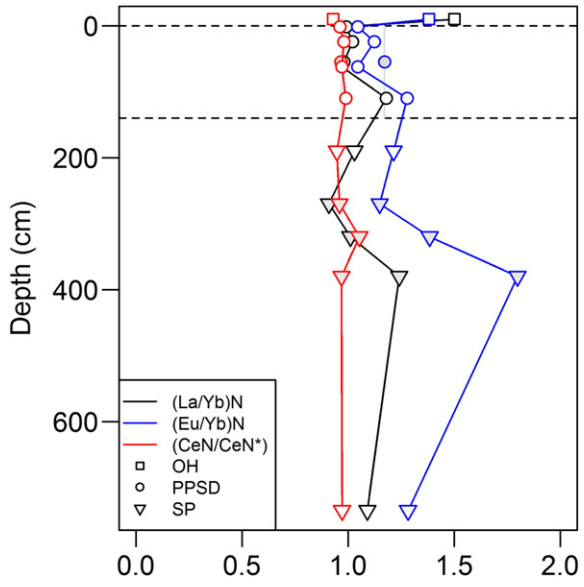

Fig. 5. Depth dependent patterns of PAAS-normalized La_N/Yb_N and Eu_N/Yb_N ratios and Ce anomaly (Ce_N/Ce_N^*) (dashed lines: lithic discontinuities; shaded area: redox sensitive horizons).

Group II comprises Co, Ni, Cu, Zn and As, which show similar distribution patterns to P_2O_5, MnO and Fe_2O_3 with a strong enrichment at 320 cm depth (SP3) in the saprolithic material. At the same time, Group IIIa comprises U and Pr, Nd, Gd, Sm, Eu, whose depth patterns resemble those of MgO and K_2O with a strong enrichment at SP4. All of them also show high concentrations in the lowermost horizon of the PPSD. These trace elements are sensitive to being mobilised during changing redox conditions in the regolith profile, *e.g.* groundwater table fluctuations. The fractionation and mobilisation/accumulation can be either direct by valence alteration into soluble/stable forms or due to the dissolution-precipitation of Fe and Mn-(oxy)hydroxides in which these trace elements get preferentially sorbed. Of particular interest here is the slight but meaningful positive Ce anomaly that can be observed in SP3 ($Ce_N/Ce_N^* = 1.05$ compared to ratios between 0.92 and 0.98 for the other samples). During water saturation periods (winter), the anoxic conditions in the saprolite result in a reducing environment which favours the leaching of REE. In the formed solution, Ce, as the majority of the lanthanides, presents a trivalent state (3+). When the water table flows downwards (summer), water is mainly retained only at the smallest pores of the soil aggregates and in the clay fraction of the saprolithic material. Oxygen can get into the interfaces, favouring Ce^{3+} to Ce^{4+} oxidation. In these oxic conditions, Ce can precipitate as

Table 3
Sr, Nd, Pb and U radiogenic isotope ratios of all analysed regolith samples (NA: not analysed).

Sample	$^{87}Sr/^{86}Sr$	$^{143}Nd/^{144}Nd$	$^{206}Pb/^{207}Pb$	$^{234}U/^{238}U$
OH	0.72181	0.511951	1.153	0.933
PPSD1	0.73023	0.511919	1.162	NA
PPSD2	0.73399	0.511922	1.204	NA
PPSD3	0.73866	0.511923	1.215	0.961
PPSD4	0.73657	0.511931	1.220	NA
PPSDce	0.73736	NA	1.226	NA
SP1	0.74141	0.511961	1.200	0.949
SP2	0.74205	0.511927	1.202	1.053
SP3	0.73912	0.511959	1.199	1.038
SP4	0.73915	0.511983	1.206	0.953
SP5	0.74160	0.511933	1.214	0.947

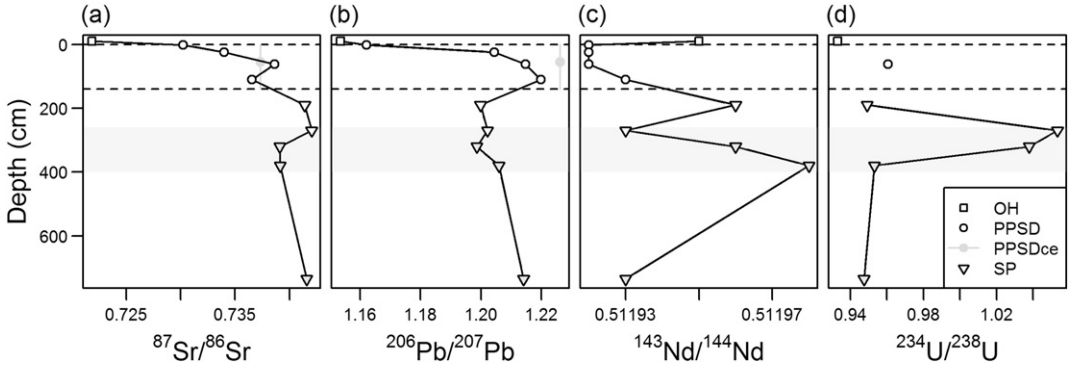

Fig. 6. Depth-dependent variation of (a) $^{206}Pb/^{207}Pb$, (b) $^{87}Sr/^{86}Sr$, (c) $^{143}Nd/^{144}Nd$ and (d) $^{234}U/^{238}U$ of all analysed samples (shaded area: redox sensitive horizons).

cerianite *e.g.* on the hydrated surface of manganese oxides (Braun et al., 1990; Steinmann and Stille, 1997). This means, in this case Ce might be mobilised from the upper horizons and immobilised at 320 cm depth. In agreement is the evolution of the U geochemistry within the studied profile (Figs. 3 and 6, and Table 2). Uranium concentrations tend to increase from 3.09 ppm at the top of the SP compartment to 5.84 ppm at SP4. Under oxidizing conditions, U can oxidise to the uranyl ion ($U(VI)O_2^{+2}$) and form compounds that are soluble in water. As with Ce, the uranyl ion can get released into the solution at SP1, migrate downwards and re-deposit as it co-precipitates with Fe oxy-hydroxides at the "summer" redox interface (SP3-SP4) (Duff et al., 2002; Bruno et al., 1995). In Fig. 6, the ($^{234}U/^{238}U$) activity ratios < 1 above SP2 (270 cm) and below SP3 (320 cm) (<0.96) but > 1 in between (>1.04) indicate, respectively, a ^{234}U depletion and enrichment of the regolith. During water-rock interaction, ^{234}U and ^{238}U have different mobilities, with a preferential leaching of ^{234}U compared to ^{238}U due to the so-called alpha recoil process (more details in *e.g.*, Chabaux et al., 2003, 2008; DePaolo et al., 2006, 2012). For a material old enough to be at secular equilibrium (*i.e.*, $^{234}U/^{238}U = 1$), such a process leads to a preferential enrichment of ^{234}U in waters compared to its parent ^{238}U, and hence to ($^{234}U/^{238}U$) activity ratios > 1 in the waters and < 1 in the residual materials (see also Schaffhauser et al., 2014; Pierret et al., 2014; Prunier et al., 2015; and references therein). Thus, during long periods of water saturation and intense weathering of the rock, ^{234}U is leached from the minerals, giving ($^{234}U/^{238}U$) activity ratios < 1 in the saprolithic materials. This seems to be the case in the studied saprolithic material above SP2 and below SP3. In the studied regolith, the water table fluctuates between 320 cm depth during low hydrological conditions and 108 cm depth during winter saturation periods (according to field monitoring hydrological data, not shown). Thus, we hypothesise that ^{234}U is mobilised above 270 cm depth and potentially accumulated around the permanent water table level (SP3–SP4), where the redox potential allows the above-mentioned co-precipitation. Conversely, the permanently saturated layer between SP3 and SP5 (735 cm) favours the downward flow of ^{234}U, whereas below SP5 depth we are on the impermeable and slightly weathered slate bedrock. This hypothesis is supported by occurrences of gleyic properties with rusty patches observed from drill cores of the saprolithic material between 340 and 380 cm depth, which correspond to strong reduction processes and iron segregation (WRB, IUSS Working Group, 2015).

In summary, the depth patterns of the Ce anomaly and ($^{234}U/^{238}U$) activity ratios together with the other redox sensitive elements, definitely point to the effect of the seasonal water table fluctuation between 108 and 380 cm depth. The regolith above SP1 is preserved from the weathering process and conserves element concentrations untouched. Whereas between SP1 and SP4, the historical exposure of the material to alternating oxic and anoxic conditions (redox conditions) favoured the dissolution-precipitation processes that control the dynamics of the redox sensitive and allied elements. Below SP4, most labile elements may be flushed away from the saprolite into deeper groundwater.

On the other hand, the behaviour of all elements from Group III in the matrix of the PPSD compartment is also related to the stability of some specific residual trace mineral phases. Zr and Hf reside in zircons, Th in monazite, Y in xenotime and Nb in Ti-bearing minerals. Similarly, PPSD4, representing the lowermost part of PPSD matrix, is enriched in LREE compared to the upper horizons (Figs. 3 and 5) pointing to an important presence of phosphate and LREE bearing trace minerals such as monazite and florencite. At last, the Eu positive anomaly of PPSD's coarse materials (PPSDce), surely relates to their greater feldspars abundance (Vázquez-Ortega et al., 2015) (Figs. 2 and 5).

Finally, vegetation life cycles (nutrition, evapotranspiration) might also have an important impact in the overall chemical composition. In this regolith, beech and oak have the greatest root density between 20 and 40 cm depth (up to 16 roots cm^{-2}). The roots uptake of macronutrients and other oligoelements is probably a major cause of element fractionation between the upper and lower PPSD layers. In this sense, *Ca* must be accumulated in the OH horizon due to biological cycling and litter decomposition (Stille et al., 2009). Phosphate concentration is high in the Ah horizon for the same reason. Then it decreases at the level of the maximum root uptake at 20 to 40 cm depth (PPSD2-3). At these depths, also Mg, K, Fe, Al and most of the REE are depleted compared to the lower PPSD4 horizon. Further studies on the vegetation are needed to better understand its geochemical impact on the regolith studied here.

5.2. Impact of atmosphere-derived anthropogenic depositions on the PPSD

The $^{87}Sr/^{86}Sr$ and $^{206}Pb/^{207}Pb$ isotope ratios decrease with decreasing depth within the organic (OH) and organo-mineral (PPSD) compartments (Fig. 6a and b and Table 3), whereas the corresponding $^{143}Nd/^{144}Nd$ ratios are only very weakly scattered, ranging between 0.51192 and 0.51195 (Fig. 6c and Table 3). The comparatively lower Pb and Sr isotopic compositions of the organic compartment (OH sample) can be related to anthropogenic impacts (Stille et al., 2011). Indeed, the current local atmospheric baseline isotopic compositions determined on lichens show significantly lower $^{206}Pb/^{207}Pb$ (1.162) and $^{87}Sr/^{86}Sr$ (0.7152) but higher $^{143}Nd/^{144}Nd$ (0.51205) ratios (Hissler et al., 2008). In a $^{87}Sr/^{86}Sr$ *vs* Rb/Sr diagram the PPSD data show a mixing trend with the OH horizon and the Ah organo-mineral soil horizon (PPSD1) with the lowest isotopic composition values and Rb/Sr ratios similar to the lichen (0.87 and 1.54 respectively) (Fig. 7a). Similar relationships are observable in the $^{206}Pb/^{207}Pb$ *vs* U/Pb diagram (Fig. 7b). Again, OH and PPSD1 samples have Pb isotopic composition and U/Pb ratios similar to lichen (U/Pb = 0.01 for both samples). Therefore, the Rb-Sr and U-Pb isotope systems of the uppermost regolith samples are strongly influenced by recent atmosphere-derived inputs. This is not the case for the Sm-Nd isotope system, which is not to be affected by atmospheric deposition (not shown). If mixing occurred between anthropogenic, atmosphere-derived and soil particles then the regolith isotope data should describe a mixing hyperbola in the $^{87}Sr/^{86}Sr$ *vs.* $^{143}Nd/^{144}Nd$

diagram (Faure, 1986). This is indeed the case (Fig. 8). The shape of the curve is controlled by the end-members Sr/Nd ratios. The atmospheric end member is the lichen (Sr: 1.17 ppm, $^{87}Sr/^{86}Sr$: 0.7152; Nd: 0.17 ppm, $^{143}Nd/^{144}Nd$: 0.51205) (Hissler et al., 2008) and the geogenic end member corresponds to the lithic material representing fresh slate bedrock (SP5) (Sr: 98.2 ppm, $^{87}Sr/^{86}Sr$: 0.7416; Nd: 37.9 ppm, $^{143}Nd/^{144}Nd$: 0.51193). The resulting Sr/Nd ratios are 6.9 for the lichen and 2.6 for the slate. One calculates that the uppermost OH and Ah horizons (PPSD1) contain up to 90% and 50% of recent atmosphere-derived Sr and 95% and 50% of recent atmosphere-derived Nd, respectively. Such enrichments are rather surprising, suggesting that these elements have been transported over distances >20 km. The closest active steel industrial parks are situated around 25 km southeast (Bissen, Luxembourg) and 120 km north-west (Liège, Belgium) of the studied site, and a historic mine of mainly Pb and Zn was located around 20 km north of the study site. Alternatively, these enrichments might be attributed to the heavy fighting nearby during the "Battle of the Bulge" in the vicinity of Bastogne during the Second World War (Cole, 1965).

5.3. Impact of volcanic events on the PPSD

In central Europe, the upper layer of PPSD (UL) often presents a typical volcanic mineralogical composition related to the Laacher See Eruption in the late Pleistocene (12,900 years BP) (Kleber and Terhorst, 2013; Semmel and Terhorst, 2010; Pissart, 1995; Wörner and Schmincke, 1984). Wörner and Schmincke (1984) and Wörner et al. (1985) also highlighted the very specific trace element and isotopical composition of the Laacher See tephra, which permits its identification and differentiation from other material contributions. These mineralogical and isotopical fingerprints allow us to use the Laacher See deposits as a stratigraphic marker (Schmincke et al., 1999). Nevertheless, relatively older volcanic events took place in the same region, such as the Rocourt (74–90.3 ka) and Eltville (16–30 ka) eruptions, whose tephras spread in the south east of Belgium, central Germany and north of Luxembourg (Pouclet and Juvigne, 2009; Pouclet et al., 2008). Pouclet et al. (2008) pointed out the potential of the Rocourt tephra as chronostratigraphic marker for the Upper Pleistocene loess deposits in these areas thanks to its glass fragment shape, chemical and mineral composition, which differs from the Laacher See tephra.

One of the principal questions raised in this study concerns the stratigraphic and pedogenetic evolution of the periglacial coverbeds (PPSD compartment) and, more specifically, the origin of their constituting mineral phases. Are these phases only derived from the underlying slate or do some of them have other origins; *e.g.* originate from volcanic dust and ashes from the late-Pleistocene Laacher See eruption, and reached also the south-western edge of the Rhenish Massif. Indeed during solifluction processes the Laacher See tephra, which was already deposited, was admixed with other materials to become part of the upper coverbed (Kleber, 1997; Schmincke et al., 1999; Semmel and Terhorst, 2010; Stückrad et al., 2010; Terhorst, 2007). Previous studies have shown that Laacher See particles have been incorporated to the upper PPSD layer in central Europe (Kleber and Terhorst, 2013; Pissart, 1995; Semmel and Terhorst, 2010). At the same time, several tephra layers have been recognized in the Upper Pleistocene Loess deposits in Belgium, as the ones of the above mentioned Laacher See, Eltville and Rocourt (Pouclet and Juvigne, 2009). Among those tephra sequences, Wörner and Wright (1984) noticed that the Laacher See tephra has a phonolite-like mineral composition dominated by alkali feldspar, especially sanidine phenocrysts, followed by plagioclase (mainly albite), haüyne, amphibole, clinopyroxene, sphene, Ti-magnetite, apatite, phlogopite and traces of zircon phenocrysts. The abundance of the different observed mineral phases of the studied regolith vary along the profile but manifest specific mineral enrichments in the matrix of the basal layer of PPSD (PPSD3 and PPSD4), which might be related to a Pleistocene eruption (Fig. 2).

In that regard, of great importance is the finding of chamosite as a main mineral phase (up to 20 vol.%) in the matrix of the basal layer of the PPSD compartment. It is significantly less present in the saprolithic material (SP, 10–13 vol.%). This mineral phase is the Fe-rich end-member of the chlorite group. Its presence explains the rather high Fe_2O_3 contents (7–11 wt.%) in the basal layer of PPSD. Chamosite is typically a replacement mineral phase and alteration product of ferromagnesian minerals such as pyroxenes and amphiboles (Deer et al., 1974). However, also other mineral phases confirm the presence of tephra in the basal layer of PPSD, such as kaolinite, which results from feldspar alteration and reaches 20 vol% which represents a strong enrichment compared to the underlying saprolite (SP, 3–5 vol%). Primary feldspar minerals such as albite and orthoclase are also observable in smaller quantities in the PPSD. Orthoclase, respectively sanidine (a not distinguishable polymorph of orthoclase), occurs only in PPSD (up to 8 vol.% in the matrix and 14 vol.% in the coarse materials) and is not at all observable in SP.

In a similar way, one might suggest that the titanium enrichments observed for the same PPSD samples (Fig. 3) result from sphene and Ti-magnetite. Indeed, the important presence of Ti-bearing minerals such as ilmenite, rutile and Ti-magnetite observed under the scanning electron microscope (SEM) confirm the presence of tephra-derived mineral constituents in the PPSD.

The deposited tephra dust particles caused elevated Nb concentrations in the samples (Schmincke et al., 1999; Haase et al., 2007) because the erupted tephra (Lower Laacher See Tephra deposits, LLST) is enriched in Nb with concentrations of >200 ppm (Wörner and Schmincke, 1984). The Nb concentrations of the studied coverbed matrix are well correlated with TiO_2 (Table 2) indicating, as suggested (Bonjour and Dabard, 1991), that titaniferous mineral phases are the principal Nb carrying phases. Nb concentrations vary according to

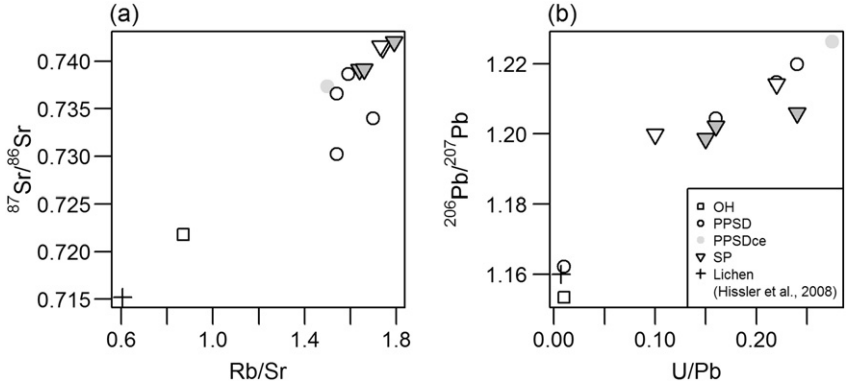

Fig. 7. Relationships between (a) $^{87}Sr/^{86}Sr$ *vs.* Rb/Sr ratio and (b) $^{206}Pb/^{207}Pb$ *vs.* U/Pb ratio of all analysed samples and a lichen sample from Hissler et al. (2008) representing the anthropogenic end member.

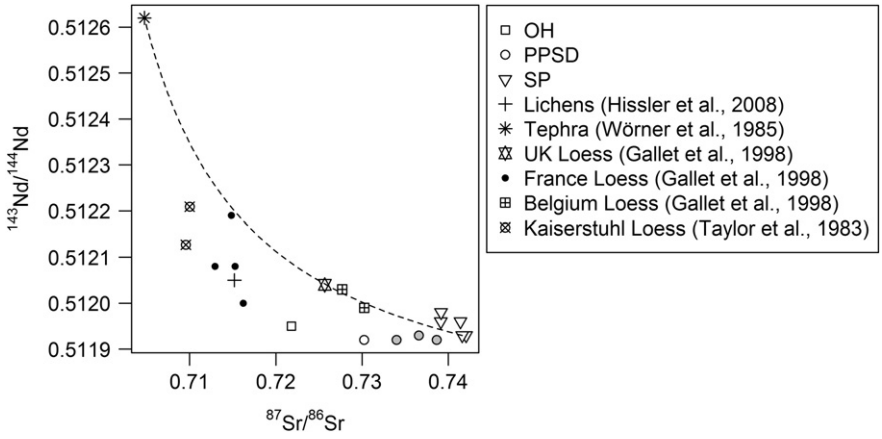

Fig. 8. $^{87}Sr/^{86}Sr$ *vs.* $^{143}Nd/^{144}Nd$ diagram describing mixing hyperbolas between the unweathered slate sample of this study (SP5) as the continental crust end member (Sr: 98.2 ppm, $^{87}Sr/^{86}Sr$: 0.7416; Nd: 37.9 ppm, $^{143}Nd/^{144}Nd$: 0.51193) and a mantle representing end member according to the study of Wörner et al. (1985) (Sr: 500 ppm; $^{87}Sr/^{86}Sr$: 0.70477; Nd: 49 ppm; $^{143}Nd/^{144}Nd$: 0.51262); and between SP5 and the lichen representing the atmospheric derived anthropogenic end member (Sr: 1.17 ppm, $^{87}Sr/^{86}Sr$: 0.7152; Nd: 0.17 ppm, $^{143}Nd/^{144}Nd$: 0.51205, from Hissler et al., 2008). Included are the loess signatures from UK, France and Belgium from Gallet et al. (1998) and Kaiserstuhl (Germany) from Taylor et al. (1983) (grey circles: Nb enriched PPSD samples).

depth, being lowest close to the surface (10.28 ppm) (Fig. 3 and Table 2). Between PPSD2 and PPSD4, the Nb concentrations range between 19.4 and 19.9 ppm and are higher than those of the underlying bedrock showing concentrations between 14 and 16 ppm. The Nb concentrations of coverbeds from two other sites of the studied plateau range, at same depths as PPSD2 to PPSD4, between 18.5 and 22.5 ppm (not shown). In the coarser materials (PPSDce) of these horizons and in the underlying bedrock, Nb concentrations decrease again to values below 11 and 16.6 ppm respectively. According to Taylor and McLennan (1985) the UCC Nb concentration is higher (25 ppm) and, therefore, the PPSD samples show Nb depletions similar to European loess studied by Gallet et al. (1998). These authors provided plausible arguments that the depletions are artefacts resulting from an over-estimation of the UCC Nb concentration. Similarly Condie (1993) suggest that the Nb concentrations of clastic sediments are seldom higher than 15 ppm. This value is in agreement with the Nb concentrations found in the bedrock below the coverbed. Thus, the fact that the PPSD matrix shows slightly higher Nb concentrations than the PPSD coarse materials and the bedrock is suggested to be the result of deposition of Nb-enriched mineral phases from the late-Pleistocene Laacher See eruption.

The Nb contribution from this eruption to the loess component of the PPSD sediments can be estimated by using a two component mixing equation, a Nb concentration of the Laacher See tephra (100 ppm) (Wörner and Schmincke, 1984) for the volcanic mixing end-member and a Nb concentration of the underlying bedrock (15 ppm) for the PPSD end-member. This rough estimation indicates that the volcanic Nb contribution is <6% in the PPSD matrix. Mixing calculations can also be performed by using Nd concentrations and $^{143}Nd/^{144}Nd$ isotope ratios (see Faure, 1986). However, the Sr-Nd isotopic and concentration similarities between slate bedrock and PPSD samples and, thus, the resulting mixing relationships (Fig. 8) suggest that the PPSD below 45 cm depth do not contain visible amounts of tephra-derived Sr and Nd. Thus, in the case of our study only Nb enrichments and mineralogical composition allow the identification of tephra contributions in the lowermost PPSD horizons. Given the fractionation of some minerals and trace elements within the PPSD, we propose that the discontinuities observed from PPSD2 and PPSD3 respond both to the impact of volcanic depositions and pedogenetic processes such as neoformation of minerals.

5.4. Impact of the saprolite (SP) on PPSD

With the exception of the two uppermost soil horizons (OH and Ah), no impact of anthropogenic Sr and Nd is observable for the rest of the regolith compartments. Similarly we have seen that neither Sr nor Nd isotope ratios are impacted by tephra depositions during Pleistocene volcanic eruption events. PPSD and SP material are isotopically very similar pointing to similar origins. This is confirmed by the major element concentrations of the slate saprolithic material (SP) and the coverbeds (PPSD) below the OH horizon, which scatter in nearly the same range (Fig. 3) and show similar depletions and enrichments compared to the reference slate layer of SP (Fig. 4). Only very few trace elements such as Nb and some redox-sensitive elements manifest, as discussed above, differences between PPSD and underlying saprolithic material. Consequently, if the PPSD profile contains, as suggested for other neighboured coverbeds (Stückrad et al., 2010), pre-industrial atmosphere-derived particles, then they have not travelled long distances but originate from the slate of the region. In Fig. 9, the εNd (T) values of the Devonian slates of our study site ("initial" epsilon Nd values, calculated back to the stratigraphic age) are plotted *versus* their stratigraphic age and compared with other European phanerozoic shales. This type of diagram was first used by Michard et al. (1985) in order to show that during major orogenic events sediments have been impacted by mantle-derived material such as volcanogenic detrital material. One observes that the slates in this study show initial εNd (T) values very similar to those of other Devonian shales collected in Brittany and Wales. These sediments have been deposited in the same oceanic environment in a period between the Hercynian and Caledonian orogenesis and are not visibly impacted by volcanogenic detritus during their deposition. Volcanogenic deposits containing significant quantities of mantle-derived material are characterised by high $^{143}Nd/^{144}Nd$ isotope ratios and low $^{87}Sr/^{86}Sr$ isotope ratios, whereas crustal materials devoid of mantle-derived material have low $^{143}Nd/^{144}Nd$ isotope ratios and high $^{87}Sr/^{86}Sr$ isotope ratios (*e.g.* SP samples). Continental crust plots in function of the proportion of integrated mantle-derived Sr and Nd on a mixing hyperbola defined by the end-member compositions of continental crust and mantle (see hypothetical mixing hyperbola in Fig. 8). Thus, when comparing the regolith data of this study with European loess and tephra data from the literature, one observes that each data set has a very particular isotopic signature. Each of these coordinates plot inside or on a mixing curve ranging from mantle or anthropogenic (low $^{87}Sr/^{86}Sr$ and $^{143}Nd/^{144}Nd$ ratios) materials to crustal materials (Fig. 8). The tephra signature from Wörner et al. (1985) being the most mantle rich material. This indicates that the different loess deposits originate from very distinct rock units containing different proportions of mantle and crust material. In this context, our PPSD show Sr and Nd isotope signatures rather close to the studied slate regolith compartment than to other losses (Fig. 8), which we hypothesise reflects the genetic link of the materials of both compartments.

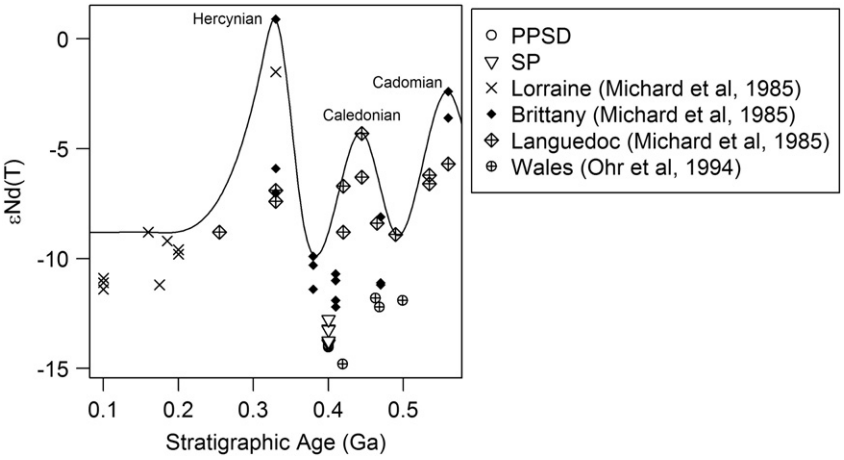

Fig. 9. εNd(T) values *vs.* stratigraphic ages of the PPSD and SP samples of this study and of rock materials which originated from similar palaeographic environments reported by Michard et al. (1985) and Ohr et al. (1994). Modified after Michard et al. (1985).

6. Conclusion

The study we performed on a typical polygenetic regolith profile from a remnant plateau from the western part of the Rhenish Massif allowed three distinct compartments to be distinguished. Their geochemical and mineralogical characteristics present contrasting evolutions, which can be related to different atmospheric deposition events and to the seasonal water saturation dynamics. The estimations based on $^{87}Sr/^{86}Sr$ and $^{143}Nd/^{144}Nd$ ratios indicate that the recent atmospheric deposition contributes to about 50% of the Sr and Nd content in the organo-mineral part of the regolith (0–45 cm depth). Nb enrichments and specific mineralogical compositions in the upper subsoil (45–140 cm depth) point to tephra contributions in the loess of the PPSD. Finally, we identified a close genetic link of both upper and lower *subsolum* materials. The fresh slate and the central European loess from the literature defines a mixing curve between crustal and mantle materials, in which our PPSD layers show signatures close to the studied slate compartment and continental crust rather than to other European loess with lower Sr and higher Nd isotopic compositions.

The combination of mineralogical, major and trace element pattern and Sr-Nd-Pb-U isotope ratio analyses appears to be an extremely powerful approach for understanding the evolution of the polygenetic regolith systems. This procedure offers the possibility of i) characterising and tracking the origin of the components that constitute the different compartments of the regolith; ii) identifying the genetic links between the different regolith compartments; and iii) doing further research on its great potential for the identification of important hydrological tracers, which are able to shed light on water pathways and water-rock interactions within the complex regolith system of the critical zone.

Acknowledgement

This study is part of a project financed by the National Research Fund (FNR) of the Grand Duchy of Luxembourg (AFR Grant 9188481). We want to thank Jean François Iffly, François Barnich and Johanna Ziebel for their help in the field and laboratories and Francis Huguet for his scientific advice. We also thank Richard Coupe from the USGS for a preliminary review of the manuscript, as well as Markus Egli, editor of the journal, and the reviewers for their helpful revision.

References

AG (Ad-hoc-Arbeitsgruppe) Boden, 2005. Bodenkundliche Kartieranleitung. E. Schweizerbart, Hannover.

Aubert, D., Stille, P., Probst, A., 2001. REE fractionation during granite weathering and removal by waters and suspended loads: Sr and Nd isotopic evidence. Geochim. Cosmochim. Acta 65, 387–406. http://dx.doi.org/10.1016/S0016-7037(00)00546-9.

Aubert, D., Stille, P., Probst, A., Gauthier-lafaye, F., Pourcelot, L., Del Nero, M., 2002. Characterization and migration of atmospheric REE in soils and surface waters. Geochim. Cosmochim. Acta 66, 3339–3350. http://dx.doi.org/10.1016/S0016-7037(02)00913-4.

Banwart, S., Bernasconi, S.M., Bloem, J., Blum, W., Brandao, M., Brantley, S., Chabaux, F., Duffy, C., Kram, P., Lair, G., Lundin, L., Nikolaidis, N., Novak, M., Panagos, P., Ragnarsdottir, K.V., Reynolds, B., Rousseva, S., de Ruiter, P., van Gaans, P., van Riemsdijk, W., White, T., Zhang, B., 2011. Soil processes and functions in critical zone observatories: hypotheses and experimental design. Vadose Zone J. 10, 974–987.

Barbier, F., 2012. Etude de paléoaltération météorique (Crétacé Inférieur à Néogène) sur socle silicoclastique hétérogène: caractérisation et essai de cartographie d'altérites en Région Wallonne (Belgique). Ph D Thesis. Prom, Yans, Johan.

Berner, R.A., Maasch, K.A., 1996. Chemical weathering and controls on atmospheric 0_2 and CO_2: fundamental principles were enunciated by J.J. Ebelmen in 1845. Geochim. Cosmochim. Acta. 60, 1633–1637.

Bini, C., Sartori, G., Wahsha, M., Fontana, S., 2011. Background levels of trace elements and soil geochemistry at regional level in NE Italy. J. Geochemical Explor. 109, 125–133. http://dx.doi.org/10.1016/j.gexplo.2010.07.008.

Bonjour, J.-L., Dabard, M.-P., 1991. Ti/Nb ratios of clastic terrigenous sediments used as an indicator of provenance. Chem. Geol. 91, 257–267. http://dx.doi.org/10.1016/0009-2541(91)90003-A.

Braun, J.-J., Pagel, M., Muller, J.-P., Bilong, P., Michard, A., Guillet, B., 1990. Cerium anomalies in lateritic profiles. Geochim. Cosmochim. Acta 54, 781–795. http://dx.doi.org/10.1016/0016-7037(90)90373-S.

Bruno, J., De Pablo, J., Duro, L., Figuerola, E., 1995. Experimental study and modeling of the U(VI)-Fe(OH)3 surface precipitation/coprecipitation equilibria. Geochim. Cosmochim. Acta 59, 4113–4123. http://dx.doi.org/10.1016/0016-7037(95)00243-S.

Catt, J.A., 1986. Soils and quaternary geology. A Handbook for Field Scientist 1986. Oxford Sciences Publications, Clarendon Press, Oxford.

Chabaux, F., O'Nions, R.K., Cohen, A.S., Hein, J.R., 1997. ^{238}U-^{234}U-^{230}Th disequilibrium in Fe-Mn crusts: palaeoceanographic record or diagenetic alteration? Geochim. Cosmoch. Acta 61, 3619–3632.

Chabaux, F., Riotte, J., Dequincey, O., 2003. U–Th–Ra fractionation during weathering and river transport. Rev. Mineral. Geochem. 52, 533–576.

Chabaux, F., Bourdon, B., Riotte, J., 2008. Chapter 3 U-series geochemistry in weathering profiles, river waters and lakes. In: Krishnaswami, S., Cochran, J.K. (Eds.), Radioactivity in the Environment. Elsevier, pp. 49–104.

Chauvel, C., Garçon, M., Bureau, S., Besnault, A., Jahn, B., Ding, Z., 2014. Constraints from loess on the Hf–Nd isotopic composition of the upper continental crust. Earth Planet. Sci. Lett. 388, 48–58. http://dx.doi.org/10.1016/j.epsl.2013.11.045.

Cole, H.M., 1965. The Ardennes: Battle of the Bulge. Vol. 8. Government Printing Office.

Condie, K.C., 1993. Chemical composition and evolution of the upper continental crust: contrasting results from surface samples and shales. Chem. Geol. 104, 1–37. http://dx.doi.org/10.1016/0009-2541(93)90140-E.

Craig, M.A., Wilford, J.R., Tapley, I.J., 1999. Regolith-landform mapping in the Gawler craton. MESA J. 12, 17–21.

Debajyoti, P., White, W.M., Turcotte, D.L., 1967. Modelling isotopic evolution of Earth. Br. Med. J. 4, 438.

Deckers, J., 1966. Contribution à l'étude de la composition et de la capacité de production des sols de l'Ardenne centrale et de la Famenne orientale. Mémoire n°3. Société belge de Pédologie, Gand, Belgique.

Deer, W.A., Howie, R.A., Zussmann, J., 1974. An Introduction to the Rock-forming Minerals. Longman, London.

Demoulin, A., 2003. Paleosurfaces and residual deposits in Ardenne-Eifel: historical overview and perspectives. Géol. Fr. 2003 (1), 17–21.

Deniel, C., Pin, C., 2001. Single-stage method for the simultaneous isolation of lead and strontium from silicate samples for isotopic measurements. Anal. Chim. Acta 426, 95–103. http://dx.doi.org/10.1016/S0003-2670(00)01185-5.

DePaolo, D.J., Maher, K., Christensen, J.N., McManus, J., 2006. Sediment transport time measured with U-series isotopes: results from ODP North Atlantic drift site 984. Earth Planet. Sci. Lett. 248, 394–410.

DePaolo, D.J., Lee, V.E., Christensen, J.N., Maher, K., 2012. Uranium comminution ages: sediment transport and deposition time scales. Compt. Rendus Geosci. 344, 678–687.
Dequincey, O., Chabaux, F., Clauer, N., Sigmarsson, O., Liewig, N., Leprun, J.C., 2002. Chemical remobilizations in laterites: evidence from trace elements and ^{238}U-^{234}U-^{230}Th disequilibria. Geochim. Cosmoch. Acta 66, 1197–1210.
Désiré-Marchand, J., 1985. Notice de la carte géomorphologique du Grand-Duché de Luxembourg. Service Géologique de Luxembourg, Bulletin. 13 (47 p).
Dietze, M., Kleber, A., 2010. Characterisation and Prediction of Thickness and Material Properties of Periglacial Cover Beds, Tharandter Wald, Germany, Geoderma. Volume 156 pp. 346–356 Issues 3–4.
Doucelance, R., Manhès, G., 2001. Reevaluation of precise lead isotope measurements by thermal ionization mass spectrometry. Chem. Geol. 176, 361–377.
Duff, M.C., Coughlin, J.U., Hunter, D.B., 2002. Uranium co-precipitation with iron oxide minerals. Geochim. Cosmochim. Acta 66, 3533–3547. http://dx.doi.org/10.1016/S0016-7037(02)00953-5.
Eggleton, R.A., 2001. The Regolith Glossary: Surficial Geology, Soils and Landscapes. Cooperative Research Centre for Landscape Evolution and Mineral Exploration, Floreat Park, WA, Canberra (144p).
FAO, 2006. Guidelines for Soil Description. fourth ed. FAO, Rome, p. 97.
Faure, G., 1986. Principles of Isotope Geology. John Wiley and Sons, Inc., New York, NY.
Felix-Henningsen, P., 1994. Mesozoic tertiary weathering and soil formation on slates of the Rhenish Massif (Germany). Catena 21, 229–242.
Field, J.P., Breshears, D.D., Law, D.J., Villegas, J.C., Lopez-Hoffman, L., Brooks, P.D., Chorover, J., Barron-Gafford, G.A., Gallery, R.E., Litvak, M.E., Lybrand, R.A., McIn-tosh, J.C., Meixner, T., Niu, G.Y., Papuga, S.A., Pelletier, J.D., Rasmussen, C.R., Troch, P.A., 2015. Critical zone services: expanding context, constraints, and currency beyond ecosystem services. Vadose Zone J. 14. http://dx.doi.org/10.2136/vzj2014.10.0142.
Gabrielli, C.P., Mcdonnell, J.J., 2012. An inexpensive and portable drill rig for bedrock groundwater studies in headwater catchments. Hydrol. Process. 26, 622–632. http://dx.doi.org/10.1002/hyp.8212.
Gallet, S., Jahn, B., Van Vliet Lanoë, B., Dia, A., Rossello, E., 1998. Loess geochemistry and its implications for particle origin and composition of the upper continental crust. Earth Planet. Sci. Lett. 156, 157–172. http://dx.doi.org/10.1016/S0012-821X(97)00218-5.
Geagea, M.L., Stille, P., Millet, M., Perrone, T., 2007. REE characteristics and Pb, Sr and Nd isotopic compositions of steel plant emissions. Sci. Total Environ. 373, 404–419. http://dx.doi.org/10.1016/j.scitotenv.2006.11.011.
Gourdol, L., Hissler, C., Hoffmann, L., Pfister, L., 2013. On the potential for the Partial Triadic Analysis to grasp the spatio-temporal variability of groundwater hydrochemistry. Appl. Geochem. 39, 93–107. http://dx.doi.org/10.1016/j.apgeochem.2013.10.002.
Granet, M., Chabaux, F., Stille, P., Dosseto, A., France-Lanord, C., Blaes, E., 2010. U-series disequilibria in suspended river sediments and implication for sediment transfer time in alluvial plains: the case of the Himalayan rivers. Geochim. Cosmochim. Acta 74, 2851–2865.
Guéguen, F., Stille, P., Dietze, V., Gieré, R., 2012. Chemical and isotopic properties and origin of coarse airborne particles collected by passive samplers in industrial, urban, and rural environments. Atmos. Environ. 62, 631–645. http://dx.doi.org/10.1016/j.atmosenv.2012.08.044.
Güler, C., Thyne, G.D., McCray, J.E., Turner, K.a., 2002. Evaluation of graphical and multivariate statistical methods for classification of water chemistry data. Hydrogeol. J. 10, 455–474. http://dx.doi.org/10.1007/s10040-002-0196-6.
Haase, D., Fink, J., Haase, G., Ruske, R., Pécsi, M., Richter, H., Altermann, M., Jäger, K.D., 2007. Loess in Europe-its spatial distribution based on a European Loess Map, scale 1:2,500,000. Quat. Sci. Rev. 26, 1301–1312. http://dx.doi.org/10.1016/j.quascirev.2007.02.003.
Hartigan, J., 1975. Clustering Algorithms. John Wiley and Sons, NY.
Hissler, C., Probst, J.-L., 2006. Impact of mercury atmospheric deposition on soils and streams in a mountainous catchment (Vosges, France) polluted by chlor-alkali industrial activity: the important trapping role of the organic matter. Sci. Total Environ. 361, 163–178. http://dx.doi.org/10.1016/j.scitotenv.2005.05.023.
Hissler, C., Stille, P., Krein, A., Geagea, M.L., Perrone, T., Probst, J.L., Hoffmann, L., 2008. Identifying the origins of local atmospheric deposition in the steel industry basin of Luxembourg using the chemical and isotopic composition of the lichen *Xanthoria parietina*. Sci. Total Environ. 405, 338–344. http://dx.doi.org/10.1016/j.scitotenv.2008.05.029.
Hissler, C., Stille, P., Juilleret, J., Iffly, J.F., Perrone, T., Morvan, G., 2015. Elucidating the formation of terra fuscas using Sr–Nd–Pb isotopes and rare earth elements. Appl. Geochemistry 54, 85–99. http://dx.doi.org/10.1016/j.apgeochem.2015.01.011.
Huguet, F., 1998. Le Hunsrück: un jalon dans l'évolution géomorphologique de la chaîne varisque/Between Hohes Venn and Schwartzwald, geomorphological investigations in Hunsrück (Rhenish Massif). Géomorphologie: relief, processus, environnement. 4, pp. 233–250 n°3.
IUSS Working Group WRB, 2015. World Reference Base for Soil Resources 2014, Update 2015. International Soil Classification System for Naming Soils and Creating Legends for Soil Maps. World Soil Resources Reports No. 106. FAO, Rome.
Jabiol, B., Zanella, A., Ponge, J.F., Sartori, G., Englisch, M., van Delft, B., de Waal, R., Le Bayon, R.C., 2013. A proposal for including humus forms in the World Reference Base for Soil Resources (WRB-FAO). Geoderma 192, 286–294. http://dx.doi.org/10.1016/j.geoderma.2012.08.002.
Juilleret, J., Iffly, J.-F., Pfister, L., Hissler, C., 2011. Remarkable Pleistocene periglacial slope deposits in Luxembourg (Oesling): pedological implication and geosite potential. Bull. Soc. Nat. Luxemb. 112, 125–130.
Juilleret, J., Dondeyne, S., Vancampenhout, K., Deckers, J., Hissler, C., 2016. Mind the gap: a classification system for integrating the subsolum into soil surveys. Geoderma http://dx.doi.org/10.1016/j.geoderma.2015.08.031.
Kaufman, L., Rouseeuw, P.J., 1990. Finding Groups in Data. John Wiley and Sons Inc., NY.
Kaufman, L., Rousseeuw, P.J., 2005. Finding Groups in Data. John Wiley and Sons Inc., NY (368pp).
Kleber, A., 1997. Cover-beds as soil parent materials in midlatitude regions. Catena 30, 197–213. http://dx.doi.org/10.1016/S0341-8162(97)00018-0.
Kleber, A., Terhorst, B., 2013. Mid-latitude slope deposits (cover beds), developments in sedimentology. Developments in Sedimentology. Elsevier http://dx.doi.org/10.1016/B978-0-444-53118-6.00001-5.
Kwaad, F.J.P.M., Mücher, H.J., 1977. The evolution of soils and slope deposits in the Luxembourg Ardennes near Wiltz. Geoderma 17, 1–37. http://dx.doi.org/10.1016/0016-7061(77)90002-7.
Levitan, D.M., Zipper, C.E., Donovan, P., Schreiber, M.E., Seal, R.R., Engle, M.a., Chermak, J.a., Bodnar, R.J., Johnson, D.K., Aylor, J.G., 2015. Statistical analysis of soil geochemical data to identify pathfinders associated with mineral deposits: an example from the Coles Hill uranium deposit, Virginia. USA. J. Geochemical Explor. 154, 238–251. http://dx.doi.org/10.1016/j.gexplo.2014.12.012.
Lin, X., Wang, X., Zhang, B., Yao, W., 2014. Multivariate analysis of regolith sediment geochemical data from the Jinwozi gold field, north-western China. J. Geochemical Explor. 137, 48–54. http://dx.doi.org/10.1016/j.gexplo.2013.11.006.
Lorz, C., Phillips, J.D., 2006. Pedo-ecological consequences of lithological discontinuities in soils-examples from Central Europe. J. Plant Nutr. Soil Sci. 169, 573–581.
Michard, A., Gurriet, P., Soudant, M., Albarede, F., 1985. Nd isotopes in French Phanerozoic shales: external vs. internal aspects of crustal evolution. Geochim. Cosmochim. Acta 49, 601–610. http://dx.doi.org/10.1016/0016-7037(85)90051-1.
Müller, E.H., 1954. Die Bedeutung des eiszeitlichen Bodenfließens (Solifluktion) für die Bodenbildung im nördlichen Teil des Rheinischen Schiefergebirges. Zeitschrift für Pflanzenernährung, Düngung, Bodenkd. 65, 52–61. http://dx.doi.org/10.1002/jpln.19540650107.
National Research Council (NRC), 2001. Basic Research Opportunities in the Earth Sciences. National Academies Press, Washington, DC.
Ohr, M., Halliday, A.N., Peacor, D.R., 1994. Mobility and fractionation of rare earth elements in argillaceous sediments: Implications for dating diagenesis and low-grade metamorphism. Geochim. Cosmochim. Acta 58, 289–312. http://dx.doi.org/10.1016/0016-7037(94)90465-0.
Paepe, R., Sommé, J., 1970. Les loess et la stratigraphie du Pléistocene récent dans le nord de la France et en Belgique. Ann. Soc. Géol. Nord 90, 191–201.
Pelt, E., Chabaux, F., Innocent, C., Navarre-Sitchler, A.K., Sak, P.B., Brantley, S.L., 2008. Uranium–thorium chronometry of weathering rinds: rock alteration rate and paleo-isotopic record of weathering fluids. Earth Planet. Sci. Lett. 276, 98–105. http://dx.doi.org/10.1016/j.epsl.2008.09.010.
Pierret, M.C., Stille, P., Prunier, J., Viville, D., Chabaux, F., 2014. Chemical and U-Sr isotopic variations of stream and source waters at a small catchment scale (the Strengbach case; Vosges mountains; France). Hydrol. Earth Syst. Sci. Discuss. http://dx.doi.org/10.5194/hessd-11-3541-2014.
Pin, C., Zalduegui, J.S., 1997. Sequential separation of light rare-earth elements, thorium and uranium by miniaturized extraction chromatography: application to isotopic analyses of silicate rocks. Anal. Chim. Acta 339, 79–89. http://dx.doi.org/10.1016/S0003-2670(96)00499-0.
Pissart, A., 1995. L'Ardenne sous le joug du froid. Le modelé périglaciaire du massif ardennais. In: Demoulin, A. (Ed.), L'Ardenne, essai de Géographie physique. Département de Géographie physique, Uni. De Liège, pp. 136–154.
Pouclet, A., Juvigne, E., 2009. The Eltville tephra, a late Pleistocene widespread tephra layer in Germany, Belgium and The Netherlands; symptomatic compositions of the minerals. Geol. Belgica. 12 (1/2), 93–103.
Pouclet, A., Juvigné, E., Pirson, S., 2008. The Rocourt Tephra, a widespread 90–74 ka stratigraphic marker in Belgium. Quat. Res. 70, 105–120. http://dx.doi.org/10.1016/j.yqres.2008.03.010.
Prunier, J., Chabaux, F., Stille, P., Gangloff, S., Pierret, M.C., Viville, D., Aubert, A., 2015. Geochemical and isotopic (Sr, U) monitoring of soil solutions from the Strengbach catchment (Vosges mountains, France): evidence for recent weathering evolution. Chem. Geol. 417, 289–305. http://dx.doi.org/10.1016/j.chemgeo.2015.10.012.
Redon, P.-O., Bur, T., Guiresse, M., Probst, J.-L., Toiser, A., Revel, J.-C., Jolivet, C., Probst, A., 2013. Modelling trace metal background to evaluate anthropogenic contamination in arable soils of south-western France. Geoderma 206, 112–122. http://dx.doi.org/10.1016/j.geoderma.2013.04.023.
Reimann, C., Filzmoser, P., Garrett, R.G., Dutter, R., 2008. Statistical Data Analysis Explained: Applied Environmental Statistics with R. John Wiley and Sons Ltd., NY (343pp).
Rousseau, D.D., Ghil, M., Kukla, G., Sima, A., Antoine, P., Fuchs, M., Hatté, C., Lagroix, F., Debret, M., Moine, O., 2013. Major dust events in Europe during marine isotope stage 5 (130–74 ka): a climatic interpretation of the "markers.". Clim. Past 9, 2213–2230. http://dx.doi.org/10.5194/cp-9-2213-2013.
Rousseau, D.-D., Chauvel, C., Sima, A., Hatté, C., Lagroix, F., Antoine, P., Balkanski, Y., Fuchs, M., Mellett, C., Kageyama, M., Ramstein, G., Lang, A., 2014. European glacial dust deposits: geochemical constraints on atmospheric dust cycle modeling. Geophys. Res. Lett. 41, 7666–7674. http://dx.doi.org/10.1002/2014GL061382.
Sauer, D., 2002. Genese, Verbreitung und Eigenschaften periglaziärer Lagen im Rheinischen Schiefergebirge- anhand von Beispielen aus Westerwald. Hunsrück und Eifel. Boden u. Landschaft 36, 1–294.
Sauer, D., Felix-Henningsen, P., 2006. Saprolite, soils, and sediments in the Rhenish Massif as records of climate and landscape history. Quat. Int. 156-157, 4–12. http://dx.doi.org/10.1016/j.quaint.2006.05.001.
Sauer, D., Scholten, T., Spies, E.-D., Felix-Henningsen, P., 2002a. Pleistocene periglacial slope deposits and colluviums in the Rhenish Massif—a result of climatic changes and human landuse. In: Rubio, J.L., Morgan, R.P.C., Asins, S., Andreu, V. (Eds.), Man and Soil at the Third Millennium Vol. 1. Geoforma Ediciones/Centro de Investigaciones sobre Desertificació n, Logron¨ o, pp. 763–776.

Schaffhauser, T., Chabaux, F., Ambroise, B., Lucas, Y., Stille, P., Reuschlé, T., Perrone, T., Fritz, B., 2014. Geochemical and isotopic (U, Sr) tracing of water pathways in the granitic Ringelbach catchment (Vosges Mountains, France). Chem. Geol. 374-375, 117–127.

Schmincke, H.-U., Park, C., Harms, E., 1999. Evolution and environmental impacts of the eruption of Laacher See Volcano (Germany) 12,900 a BP. Quat. Int. 61, 61–72. http://dx.doi.org/10.1016/S1040-6182(99)00017-8.

Schot, P.P., van der Wal, J., 1992. Human impact on regional groundwater composition through intervention in natural flow patterns and changes in land use. J. Hydrol. 134, 297–313. http://dx.doi.org/10.1016/0022-1694(92)90040-3.

Scott, K.M., Pain, C.F. (Eds.), 2008. Regolith Science. Springer Science and CSIRO, Dordrecht, The Netherlands, and Collingwood, Australia.

Semmel, A., Terhorst, B., 2010. The concept of the Pleistocene periglacial cover beds in central Europe: a review. Quat. Int. 222, 120–128. http://dx.doi.org/10.1016/j.quaint.2010.03.010.

Soil Science Glossary Terms Committee (SSGT), 2008. Internet glossary of soil science terms bhttps: //www.soils.org/publications/soils-glossaryN (accessed 17.08.2015).

Steinmann, M., Stille, P., 1997. Rare earth element behavior and Pb, Sr, Nd isotope systematics in a heavy metal contaminated soil. Appl. Geochem. 12, 607–623.

Stille, P., Pierret, M.C., Steinmann, M., Chabaux, F., Boutin, R., Aubert, D., Pourcelot, L., Morvan, G., 2009. Impact of atmospheric deposition, biogeochemical cycling and water-mineral interaction on REE fractionation in acidic surface soils and soil water (the Strengbach case). Chem. Geol. 264, 173–186. http://dx.doi.org/10.1016/j.chemgeo.2009.03.005.

Stille, P., Pourcelot, L., Granet, M., Pierret, M.C., Guéguen, F., Perrone, T., Morvan, G., Chabaux, F., 2011. Deposition and migration of atmospheric Pb in soils from a forested silicate catchment today and in the past (Strengbach case): evidence from ^{210}Pb activities and Pb isotope ratios. Chem. Geol. 289, 140–153. http://dx.doi.org/10.1016/j.chemgeo.2011.07.021.

Stückrad, S., Sabel, K.J., Wilcke, W., 2010. Contributions of different parent materials in soils developed from periglacial cover-beds. Eur. J. Soil Sci. 61, 844–853. http://dx.doi.org/10.1111/j.1365-2389.2010.01288.x.

Taylor, G., Eggleton, R.A., 2001. Regolith Geology and Geomorphology 375 pp John Wiley & Sons Ltd., Chichester, New York, Weinheim, Brisbane, Singapore, Toronto.

Taylor, S.R., McLennan, S.M., 1981. The composition and evolution of the continental crust: rare earth element evidence from sedimentary rocks. Phil. Trans. R. Soc. Lond. A301, 381–399.

Taylor, S.R., McLennan, S.M., 1985. The Continental Crust: Its Composition and Evolution. Blackwell, Oxford (312p).

Taylor, S.R., McLennan, S.M., McCulloch, M.T., 1983. Geochemistry of loess, continental crust composition and crustal model ages. Geochim. Cosmochim. Acta 47, 1897–1905.

Templ, M., Filzmoser, P., Reimann, C., 2008. Cluster analysis applied to regional geochemical data: problems and possibilities. Appl. Geochemistry 23, 2198–2213. http://dx.doi.org/10.1016/j.apgeochem.2008.03.004.

Terhorst, B., 2007. Periglacial cover beds and soils in landslide areas of SW-Germany. Catena 71, 467–476. http://dx.doi.org/10.1016/j.catena.2007.03.021.

Vázquez-Ortega, A., Perdrial, J., Harpold, A., Zapata-Ríos, X., Rasmussen, C., McIntosh, J., Schaap, M., Pelletier, J.D., Brooks, P.D., Amistadi, M.K., Chorover, J., 2015. Rare earth elements as reactive tracers of biogeochemical weathering in forested rhyolitic terrain. Chem. Geol. 391, 19–32. http://dx.doi.org/10.1016/j.chemgeo.2014.10.016.

Völkel, J., Huber, J., Leopold, M., 2011. Significance of Slope Sediments Layering on Physical Characteristics and Interflow Within the Critical Zone - Examples from the Colorado Front Range, USA, Applied Geochemistry, Volume 26, Supplement, June 2011. pp. S143–S145 http://dx.doi.org/10.1016/j.apgeochem.2011.03.052 ISSN 0883-2927.

Ward, J.H., 1963. Hierarchical grouping to optimize an objective function. J. Am. Stat. Assoc. http://dx.doi.org/10.1080/01621459.1963.10500845.

West, N., Kirby, E., Bierman, P., Slingerland, R., Ma, L., Rood, D., Brantley, S., 2013. Regolith production and transport at the Susquehanna Shale Hills Critical Zone Observatory, Part 2: insights from meteoric 10 Be. J. Geophys. Res. Earth Surf. 118, 1877–1896. http://dx.doi.org/10.1002/jgrf.20121.

Wörner, G., Schmincke, H.-U., 1984. Mineralogical and chemical zonation of the Laacher See tephra sequence (East Eifel, W. Germany). J. Petrol. 25, 805–835. http://dx.doi.org/10.1093/petrology/25.4.805.

Wörner, G., Wright, T.L., 1984. Evidence for magma mixing within the Laacher See magma chamber (East Eifel, Germany). J. Volcanol. Geotherm. Res. 22, 301–327. http://dx.doi.org/10.1016/0377-0273(84)90007-6.

Wörner, G., Staudigel, H., Zindler, A., 1985. Isotopic constraints on open system evolution of the Laacher See magma chamber (Eifel, West Germany). Earth Planet. Sci. Lett. 75, 37–49. http://dx.doi.org/10.1016/0012-821X(85)90048-2.